Chapter - V
Effect of swift heavy ions on physical properties of PMMA/Ni and PS/Ni nanocomposites

Abstract

In this chapter swift heavy ions (120 MeV Si ions, 85 MeV C ions) induced modifications of Nickel nanoparticles dispersed PMMA and PS composites films at the fluences of 1 x 10^{11}, 1 x 10^{12} ions/cm^2 were studied. 120 MeV Si swift heavy ions induced more prominent effects on the physicochemical properties of polymer nanocomposites compared to those of C-ions. An XRD analysis reveals that the crystallite size of the composites decreased after ion beam irradiation which is also corroborated by the DSC analysis due to the chain scissioning upon irradiation in PMMA nanocomposites. In PS nanocomposites, we observed cross linking upon irradiation. It was observed from the UV- visible spectroscopy analysis that the band gap value moved to the lower energy on doping with metal nanoparticles, as well as upon irradiation. SEM images showed damages upon ion beam irradiation. Magnetic properties enhanced after irradiation which may be attributed to the exchange dipole interaction of particles in the matrix and generation of free radicals.The dielectric constant of the composites increased with the increase of metal content and also upon ion beam irradiation. These phenomena could be interpreted from interfacial polarization of heterogeneous systems.

5.0 Introduction:

Nanoscale materials promise to be important in the development of various current and future focused applications. New behavior at nanoscale not only arises due to the order of magnitude reduction in size but also the appearance of new characteristics like size confinement, interfacial phenomena, quantum mechanics, Coulomb blockade etc [1]. Nanoparticles are characterized by an extremely large surface to volume ratio, and their properties are determined mainly by the behavior of their surface [2]. Nanosize particles (NPs) of ferromagnetic metals such as Fe, Co, and Ni have been extensively studied due to the richness of their novel physical properties and the broad range of potential applications. As an important transition metal, Ni nanoparticles have wide range of applications in the fields of permanent magnets, magnetic fluids, magnetic recording media, solar energy absorption, fuel cell electrodes, catalysts etc [3]. Metal nanoparticles dispersed in polymer matrices have recently been the subjects of intense study for the development of nano electronics devices [4]. The thermoplastic polymers used as the hosts are the potential lead for manufacture of the nanocomposites because the size and distribution of dispersed metal nanoparticles can be readily organized.

The ion irradiated polymers exhibited enhanced oxidation resistance and improved electrical conductivity. Irradiation effects in inorganic materials are manifested as changes in physical properties such as refractive index, magnetization and hardness [5]. The fundamental processes associated with these changes are defect formation through electronic and nuclear interactions of radiation and the subsequent chemical interaction between the defects and elements in the materials. Study of radiation induced defects in inorganic compounds is important for their role in device fabrication [6, 7]. The chemical changes brought about by ion beam in polymers

underline that the physical modifications are limited to a few basic processes: gas evolution, cross linking and degradation. The chemical changes are more dramatic in polymers because of the macromolecular structure of these materials. The kind of changes, which predominate, depends on the polymer type and radiation dosage.

In this chapter we are dealing with polymer nanocomposites and effect of irradiation upon

(i) PMMA + Ni [8]

(ii) PS + Ni [9]

Properties and preparation methods of nanocomposites have been discussed in chapter 2. All the films were irradiated with 120 MeV Si- ions and 85 MeV C- ions at the fluences of 1 x 10^{11}, 1 x 10^{12} ions/cm^2 at Inter University Accelerator Centre (IUAC), New Delhi, India. We have studied changes in the optical, structural, dielectric thermal and magnetic properties of composites due to swift heavy ion irradiation by means of UV–visible spectroscopy, X-ray diffraction, impedance gain phase analyzer and differential scanning calorimetry and SQUID magnetometer.

5.1 Effect of swift heavy ions irradiation on PMMA + Ni nanocomposites:

5.1.1 X-ray diffraction analysis:

X-ray diffraction spectra as shown in Fig. 5.1(a-g) reveal the amorphous nature of pure PMMA and crystalline behaviour of Ni powder. The appearance of sharp peak in composite indicates some degree of crystallinity, although the decrease in intensity of the diffraction peak and a slight broadening of the peak after irradiation gives evidence of decrease in crystallinity. However, no considerable change in the peak position is observed, which reveals that the lattice parameters do not change significantly [10]. The crystallite size has been calculated before and after irradiations

using Scherrer's formula [11] as dicussed in chapter 2 in section 2.3.1 from the realtion 2.2.3.

$b=K\lambda/L\cos\theta$

where b is FWHM in radians, λ is the wavelength of X-ray beam (1.5418 Å), L is the crystallite size in Å, K is a constant which varies from 0.89 to 1.39, but for most of the cases it is close to 1.

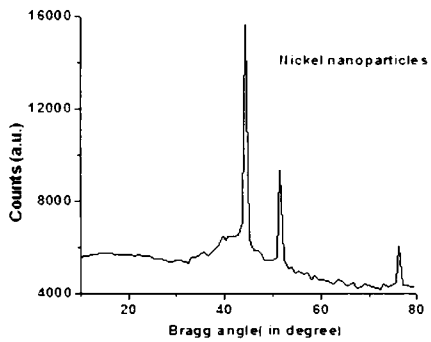

(a)

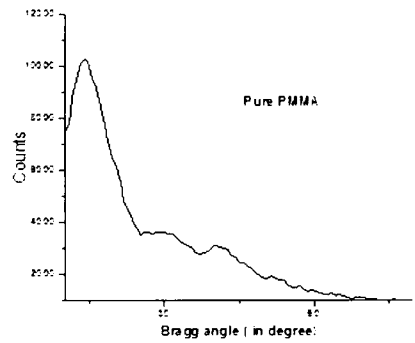

(b)

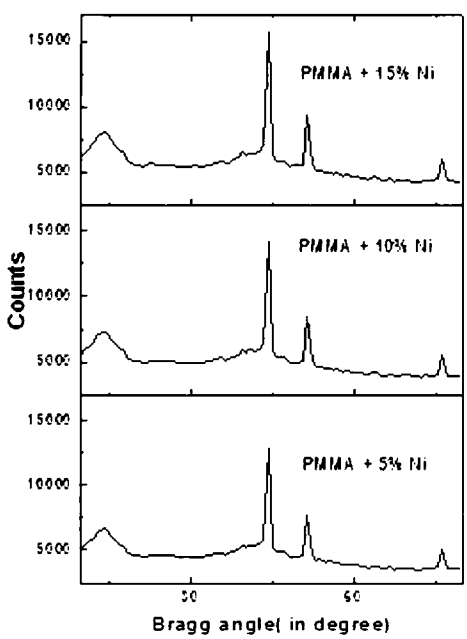

(c)

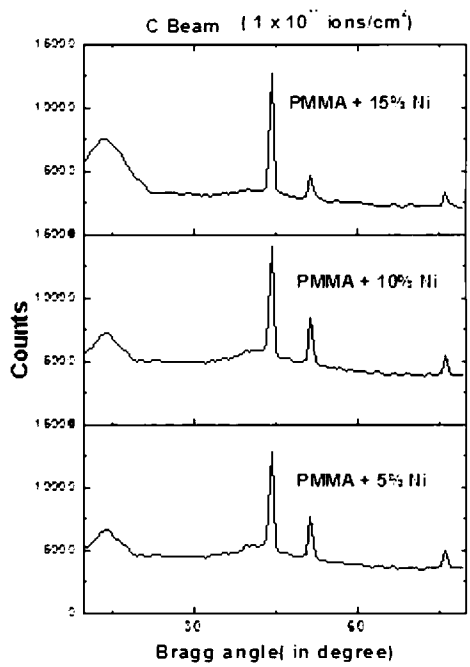

(d)

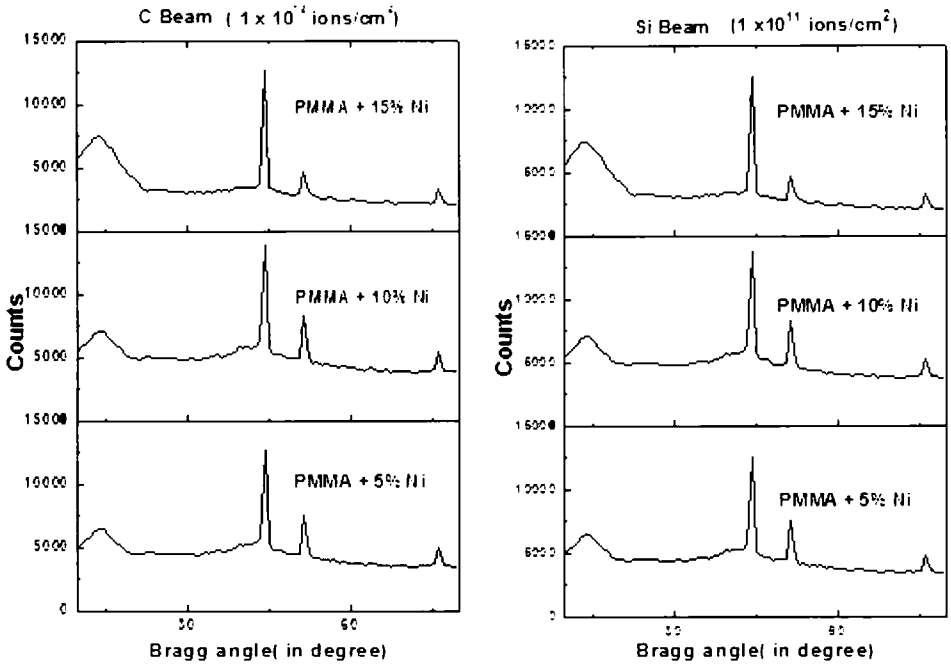

(e) (f)

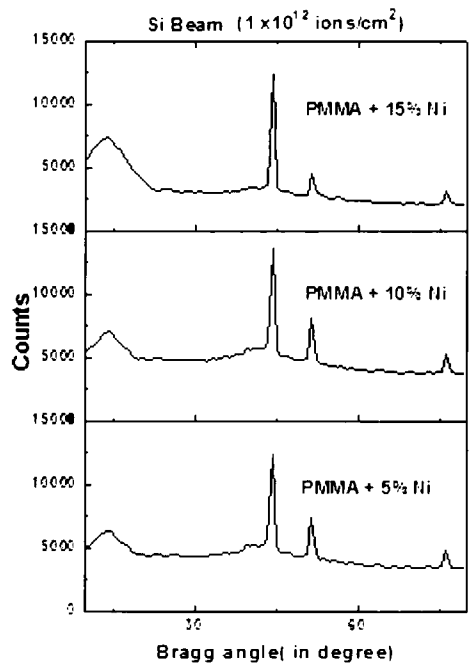

(g)

Fig. 5.1 X-ray diffraction patterns of (a) nickel nanoparticles (b) pure PMMA (c) PMMA+ Ni(pristine), (d) C beam (1×10^{11} ions/cm^2) (e) C beam (1×10^{12} ions/cm^2) (f) Si beam (1×10^{11} ions/cm^2) (g) Si beam (1×10^{12} ions/cm^2)

The crystallite sizes of the pristine and irradiated samples are listed in Table 5.1. The irradiation may induce chain scissioning, which is also corroborated by DSC analysis, assumed to be responsible for the reduction in crystallinity of the composite because of large amount of energy deposition in the material [10].

Table 5.1 Crystallite size of pristine and irradiated samples

Sample	Pristine		C Beam		Si Beam	
	2θ	Crystallite size (nm)	Crystallite size (nm) ($1x10^{11}$) ions/cm^2	Crystallite size (nm) ($1x10^{12}$) ions/cm^2	Crystallite size (nm) ($1x10^{11}$) ions/cm^2	Crystallite size (nm) ($1x10^{12}$) ions/cm^2
PMMA+ 5%Ni	44.58	14.65	14.21	13.78	13.65	13.53
	51.58	12.82	12.35	11.21	11.02	10.37
	Average	13.74	13.28	12.50	12.34	11.95
PMMA + 10%Ni	44.35	14.20	13.51	12.50	12.05	11.87
	51.40	11.90	11.45	11.03	10.80	10.20
	Average	13.05	12.48	11.77	11.43	11.04
PMMA + 15%Ni	44.28	12.54	11.10	11.05	10.98	10.67
	51.37	10.50	10.32	10.21	10.04	9.58
	Average	11.52	10.71	10.63	10.51	10.13

5.1.2 Thermal response (Differential Scanning Calorimetery (DSC)):

The glass transition temperature (*T*g) is the important property of the polymer, The glass transition is defined to be the reversible change in amorphous materials between a hard, brittle state into a rubbery molten state. At the glass transition temperature, the weak secondary bonds that stick the polymer chains together are broken, and the macromolecule starts to move. A differential scanning calorimetry (DSC) experiment was performed using a reference and a predetermined heating (or cooling) rate was imposed to the system with a temperature excursion. If a temperature difference develops between the sample and reference, the power is adjusted to remove the

difference and DSC measures the heating power difference between the sample and reference and it was recorded as shown in Fig. 5.2. The pure PMMA has a Tg value of about 64.60 °C, while tendency of increasing Tg value after insertion of nanoparticles was observed for Ni/PMMA nanocomposites. We found that the value of Tg, for pristine and irradiated samples is observed at about 78.74°C and 76.33°C, respectively, for highest concentration of Ni nanoparticles due to Si ion irradaition. After irradiations, it was found that Tg shifted to lower temperature. It reveals that the ion irradiation leads to polymer chain scissioning and subsequently reduction in molecular weight. As a result, the system moved towards the more disordered state, which is also corroborated by XRD results [12]. The value of Tg for highest fluence is listed in Table5.2.

Table 5.2 Values of glass transition for pristine and irradiated composites

Sample name	Tg (Pristine)	Tg (C beam)	Tg (Si beam)
PMMA + 5 %Ni	67.1	66.5	65.1
PMMA + 10 %Ni	71.2	69.5	66.9
PMMA + 15 %Ni	77.8	76.8	72.8

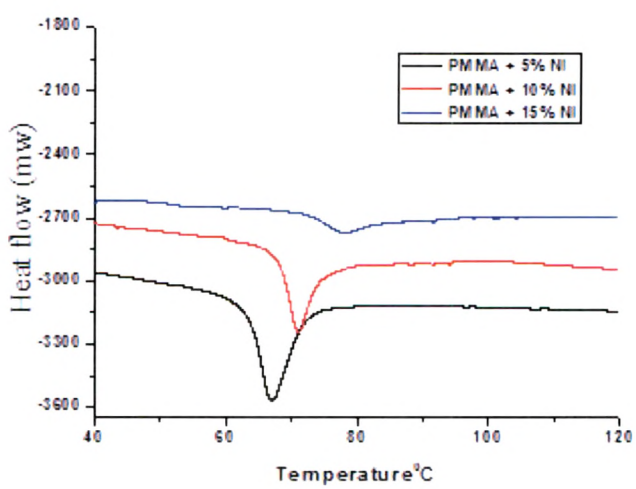

(a)

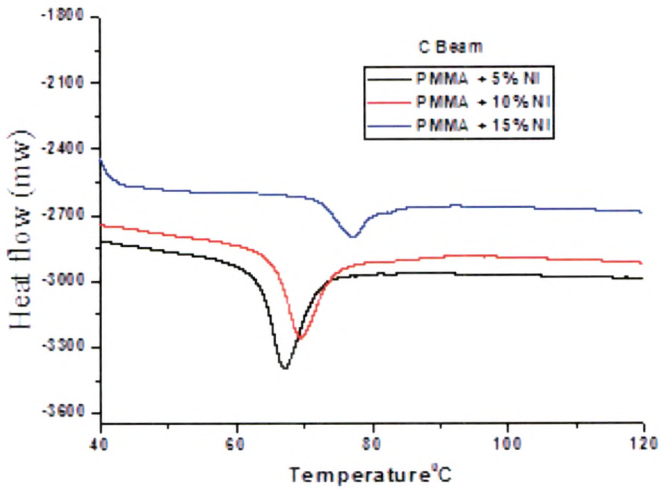

(b)

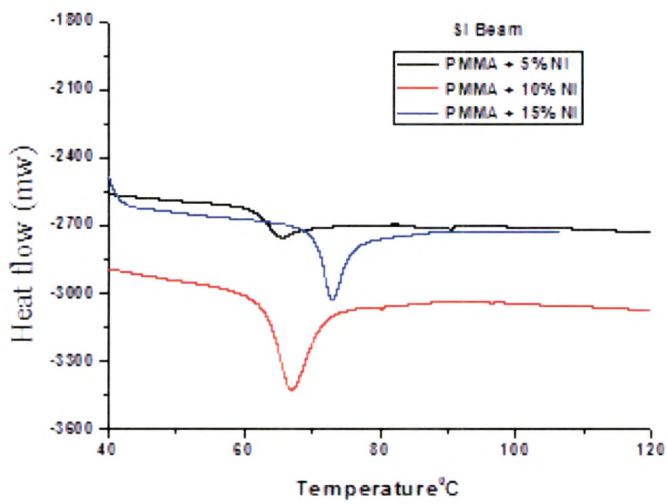

(c)

Fig. 5.2 DSC curves for pristine and irradiated (1 x10^{12} ions/cm^2) samples

5.1.3 Optical response:

The promotion of electrons in the σ, π and n orbitals from ground state to the higher energy states which are described by molecular orbitals due to the absorption of light energy by polymeric samples in the UV and visible regions. Many of the optical

transitions which occur due to the presence of impurities have energies in the visible region of the spectrum, consequently the defects are referred to as colour centres. The effect of ion beam interaction with polymers produces damage and leads to the generation of new defects and charge states [13, 14]. A shift in the absorption edge towards longer wavelength is observed for irradiated samples as shown in Fig. 5.3(a-e). This behaviour is generally interpreted as caused by the formation of extended systems of conjugated bonds, i.e. possible formation of carbon clusters. In the investigated range of wavelengths the absorption bands are associated to the π–π^* electronic transitions. These types of transitions occur in the unsaturated centers of the molecules, i.e. in compounds containing double or triple bonds and also in aromatics. The excitation of π electron requires smaller energy and hence, transition of this type occurs at longer wavelengths [15].

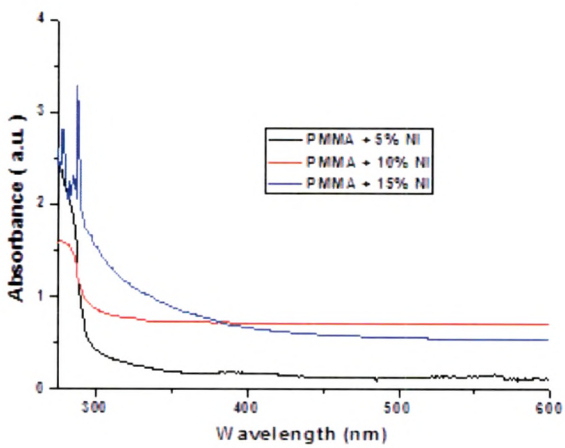

(a)

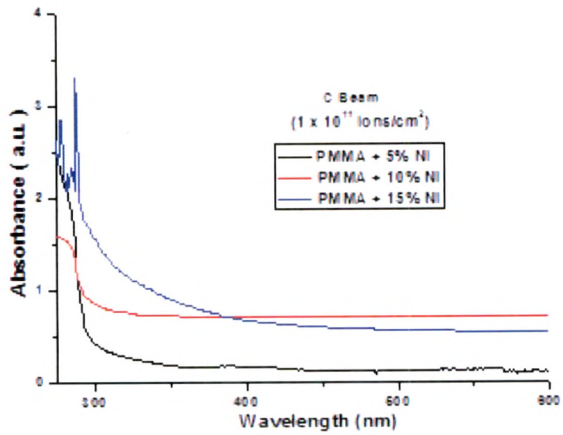
C Beam
(1 x 10^11 Ions/cm^2)
PMMA + 5% Ni
PMMA + 10% Ni
PMMA + 15% Ni
Absorbance (a.u.)
Wavelength (nm)

(b)

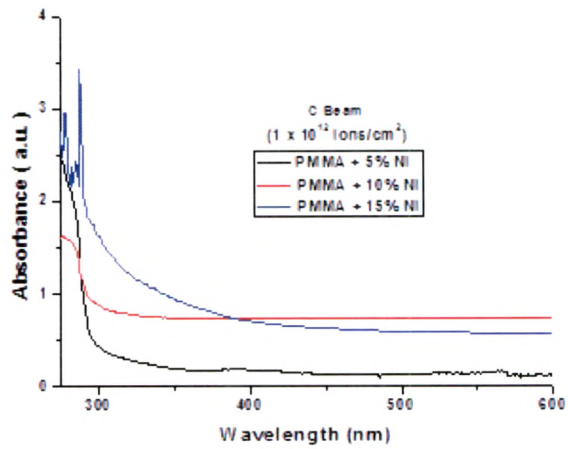
C Beam
(1 x 10^12 Ions/cm^2)
PMMA + 5% Ni
PMMA + 10% Ni
PMMA + 15% Ni
Absorbance (a.u.)
Wavelength (nm)

(c)

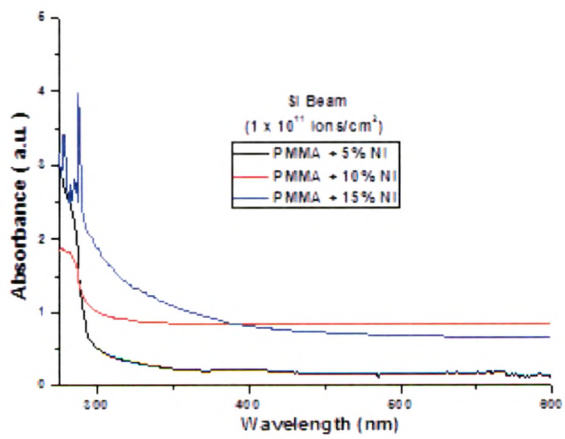
Si Beam
(1 x 10^11 Ions/cm^2)
PMMA + 5% Ni
PMMA + 10% Ni
PMMA + 15% Ni
Absorbance (a.u.)
Wavelength (nm)

(d)

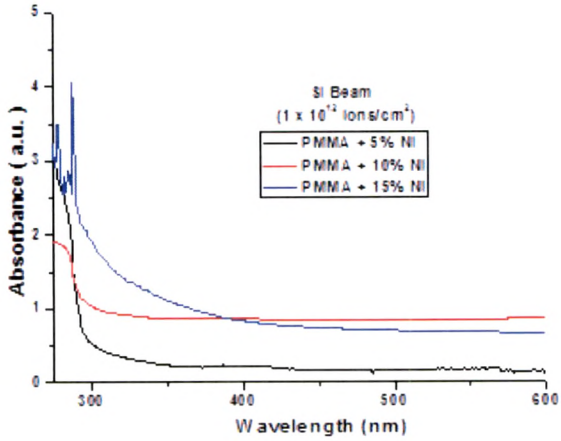

(e)

Fig. 5.3 Absorbance spectra for (a) PMMA+ Ni (pristine) (b) C beam (1 x 10^{11} ions/cm^2) (c) C beam (1 x 10^{12} ions/cm^2) (d) Si beam (1 x 10^{11} ions/cm^2) (e) Si beam (1 x 10^{12} ions/cm^2)

Determination of band gap:

The change in optical properties have been studied by Perkin- Elmer 25 Lambda UV-Visible spectrophotometer for the pristine and irradiated samples in the frequency range 200-600 cm^{-1} as illustrated in Fig. 5.3. The optical band gap E_g is obtained by Tauc's equation [16] as described in chapter 2 in section 2.3.3 by relation 2.2.4.

$\omega\varepsilon(\lambda)=(\hbar\omega-E_g)^2$

where $\varepsilon(\lambda)$ is the optical absorbance and λ is the wavelength. The intersection of the extrapolated spectrum with the abscissa of the plot $\varepsilon^{1/2}/\lambda$ versus $1/\lambda$ yields the gap wavelength λ_g from which the energy gap is derived as $E_g = hc/\lambda_g$. It is noticed that the band gap (energy gap) value shifted to lower energy from 4.37 eV to 3.43 eV due to doping of nickel nanoparticles and also upon irradiation. This is because of the scissioning of polymer chain and as a result, creation of free radicals, unsaturation etc. and thus a capability of increasing the conductivity of the composites [17].

The number of carbon atoms per cluster (N) can be calculated by following the relation 2.2.5 [18] as discussed in chapter 2 in section 2.3.3; the values are listed in Table 5.3.

$Eg=34.3/\sqrt{N}eV$

where N is the number of carbon atoms per cluster and Eg is the energy band gap.

Table 5.3 Band gap by direct allowed transitions, number of carbon atoms in pristine and irradiated composites films.

Sample	Pristine	C Beam		Si Beam	
	B.G eV	B.G eV 1×10^{11} ions/cm^2	B.G eV 1×10^{12} ions/cm^2	B.G eV 1×10^{11} ions/cm^2	B.G eV 1×10^{12} ions/cm^2
PMMA + 5%Ni	4.37	4.28	4.18	4.15	3.95
PMMA + 10%Ni	4.16	4.10	3.92	3.86	3.74
PMMA + 15%Ni	3.84	3.75	3.55	3.48	3.43

Sample	Pristine	C Beam		Si Beam	
	No. of carbon atoms(N)	No. of carbon atoms(N) 1×10^{11} ions/cm^2	No. Of carbon atoms(N) 1×10^{12} ions/cm^2	No. of carbon atoms(N) 1×10^{11} ions/cm^2	No. Of carbon atoms(N) 1×10^{12} ions/cm^2
PMMA + 5%Ni	62	64	67	68	75
PMMA + 10%Ni	68	72	77	80	84
PMMA + 15%Ni	80	83	90	97	100

5.1.4 Surface Morphology:

Fig. 5.4(a–d) shows the SEM images of pristine, composites and irradiated composite films with magnification of X250. The analysis shows that the filled partilces are distributed randomly in the matrix which display continuous contact between themselves and formed conducting paths. After irradiation, significant changes in surface morphology were observed. Considerable damage in the polymeric structure was observed after irradiation, which is also responsible for decrease in crystallinity of the material as indicated by XRD analysis [19].

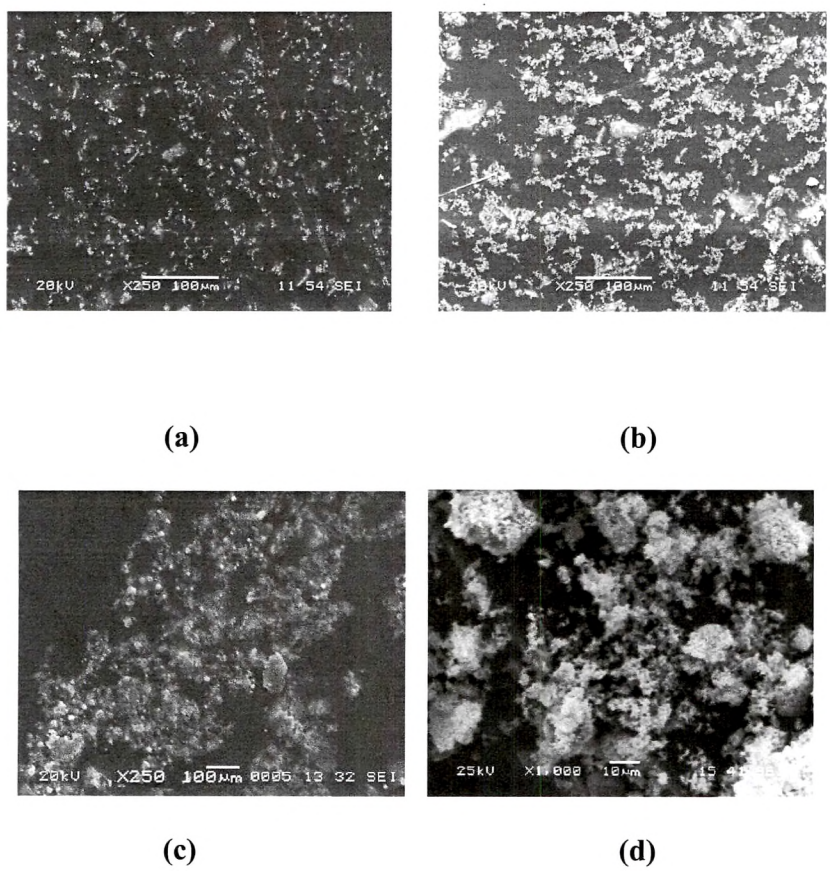

(a) **(b)**

(c) **(d)**

Fig. 5.4 SEM images of (a) PMMA+ 15 % Ni (pristine) (b) PMMA + 15 % Ni (C beam) (c) PMMA + 15 % Ni (Si beam) and (d) Nickel nanoparticles

5.1.5 Magnetic Properties:

The temperature (T) and magnetic field (H) variations of the magnetization (M) were measured with a SQUID (superconducting quantum interference device)

magnetometer. The temperature variations of M for the zero field- cooled (ZFC) and the field-cooled (FC) cases were measured from 5-300 K at applied field, H = 500 Oe. Hysteresis measurements were carried out at 300 K with magnetic field swept from 50 kOe to -50 kOe.

Nickel is known to be one of the important magnetic materials. The magnetic measurement of Ni/PMMA nanocomposites having Ni concentration of 15% by weight is discussed here. Figure 5.5(a, b, c) shows the M-H curves for the pristine and irradiated samples. The magnetic parameters extracted from the measurements are listed as saturation magnetization (M_S) ~ 0.085 emu/gm, coercive field (H_C) ~ 138 Oe, remnant magnetization (M_R) ~ 0.015 emu/gm for pristine and M_S ~ 0.107 emu/gm, H_C ~147 Oe, M_R ~ 0.020 emu/gm and M_S ~ 0.120 emu/gm, H_C ~150 Oe, M_R ~ 0.022 emu/gm for C and Si ions irradiated composites, respectively. For the sake of comparison, we note that the saturation magnetization and the coercive field for commercial bulk nickel powder at 300 K are about 57.5 emu/g and 100 Oe, respectively. Kumar et al.[20] showed that M_S ~ 30.1 emu/gm for nickel nanoparticles in the polystyrene matrix is smaller than that of commercial bulk nickel powder; the magnetization of the nickel nanoparticles in the polystyrene matrix at 1.6 Tesla did not reach full saturation and shows a very weak hysteresis. This deviation is undoubtedly a result of the nanostructure of the sample. The saturation magnetization in nanoparticle system is generally lower than that of the bulk materials and is strongly influenced by the supporting matrix. The increase in values of M_S and H_C after irradiation may be attributed to the change in exchange and dipolar interactions mediated by the matrix.

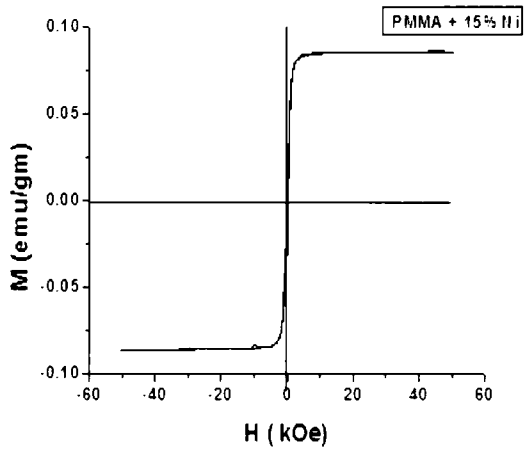
PMMA + 15% Ni
M (emu/gm)
H (kOe)

(a)

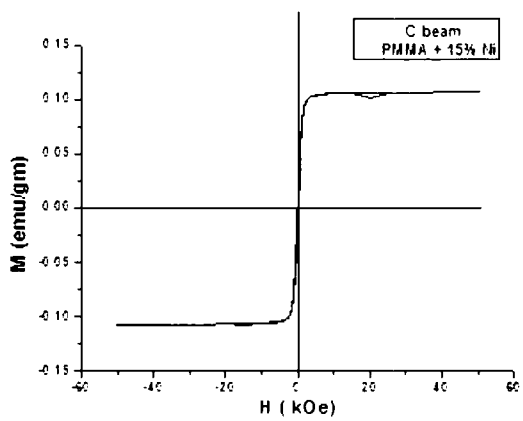
C beam
PMMA + 15% Ni
M (emu/gm)
H (kOe)

(b)

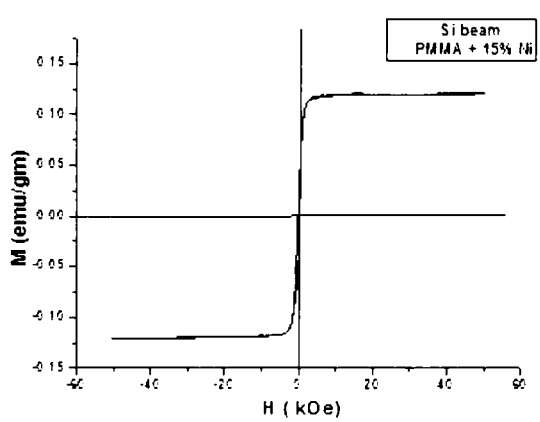
Si beam
PMMA + 15% Ni
M (emu/gm)
H (kOe)

(c)

Fig. 5.5 M-H loop for pristine and irradiated samples

Fig. 5.6 shows the comparison of FC-ZFC curves for nanocomposites. For the zero-field-cooled (ZFC) measurements, the sample was cooled down from room temperature to 5 K in the absence of an external magnetic field and the magnetic data were acquired during the warming run in a constant external field. In the field-cooled (FC) measurements, the samples were initially cooled down to 5 K in the presence of a magnetic field and the FC data were recorded during the warm up cycle in the same magnetic field.

FC magnetization decreases continuously with the increase of temperature. Such characteristic behavior of FC magnetization data is attributed to ferromagnetism in material [21]. None of these curves show any characteristic sharp change in magnetization associated with the well established ferromagnetic to super paramagnetic transition in single domain nanoparticles. This indicates that the particles (mostly in clusters) in the polymer matrix are predominantly ferromagnetic [22].

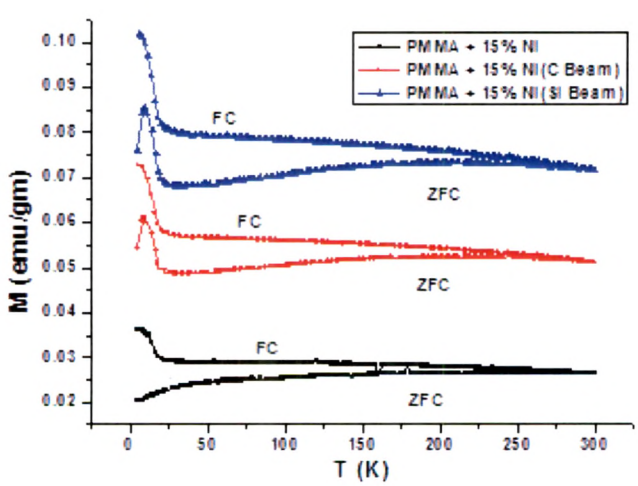

Fig. 5.6 FC- ZFC magnetization for pristine and irradited samples

5.1.6 AC Electrical Frequency Response:

Conductivity: Fig. 5.7(a-e) shows the frequency dependence of AC electrical conductivity of pristine and irradiated nanocomposites. The increase in conductivity with nickel concentration for pristine samples may be attributed to the conductive phase formed by dispersed metal nano particles in the polymer matrix. It is known that electrical conductivity of such composites depends on the type and concentration of the dispersed materials [23, 24]. An AC field applied to the metal–polymer–metal structure may cause a net polarization which is out of phase at sufficiently high frequency with the field. This may result in an increased AC conductivity which appears at frequencies greater than that at which traps are filled or emptied [25]. It is also observed that conductivity increases on increasing fluence. This increase in conductivity is probably due to the generation of large number of charged and active chemical species, cations, anions, and radicals [26].

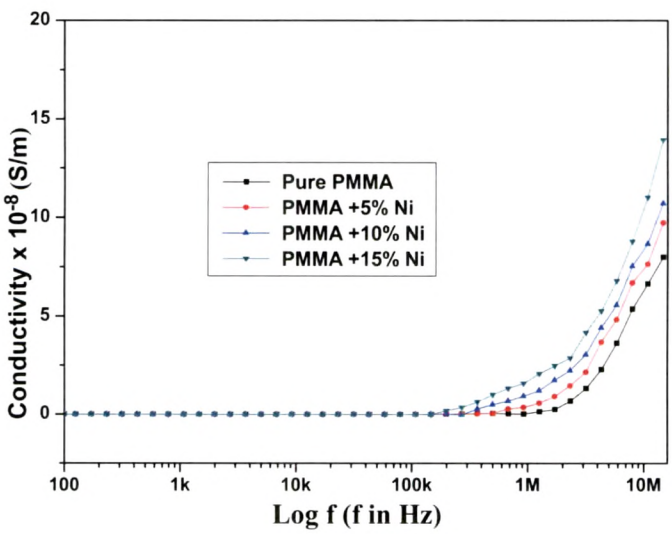

(a)

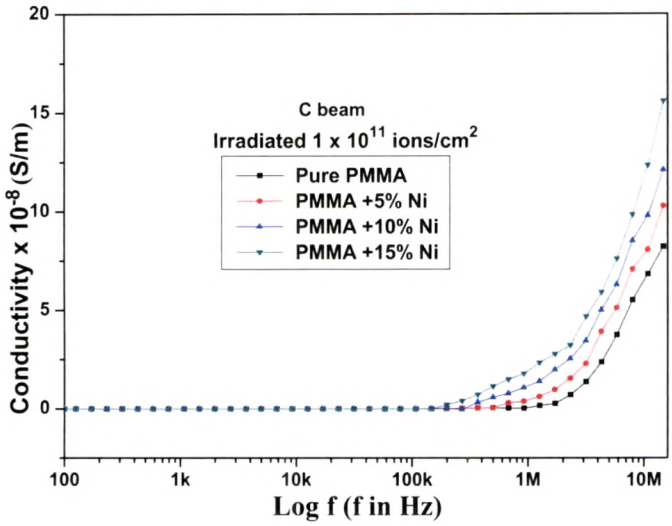
C beam
Irradiated 1 x 10^11 ions/cm^2
Pure PMMA
PMMA +5% Ni
PMMA +10% Ni
PMMA +15% Ni
Conductivity x 10^-8 (S/m)
Log f (f in Hz)
20
15
10
5
0
100
1k
10k
100k
1M
10M

(b)

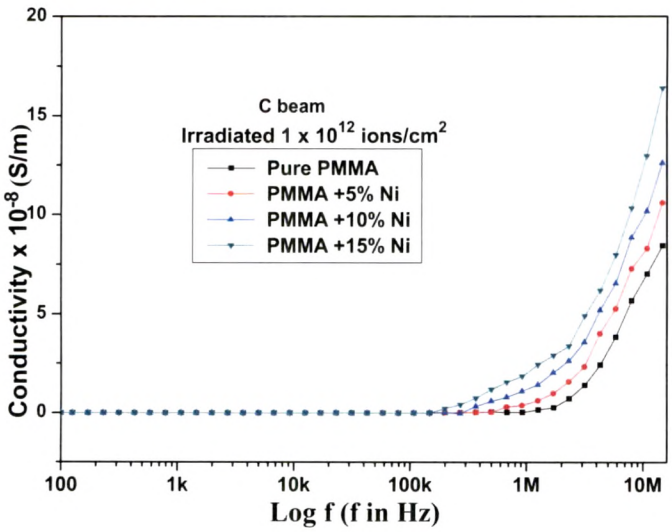
C beam
Irradiated 1 x 10^12 ions/cm^2
Pure PMMA
PMMA +5% Ni
PMMA +10% Ni
PMMA +15% Ni
Conductivity x 10^-8 (S/m)
Log f (f in Hz)
20
15
10
5
0
100
1k
10k
100k
1M
10M

(c)

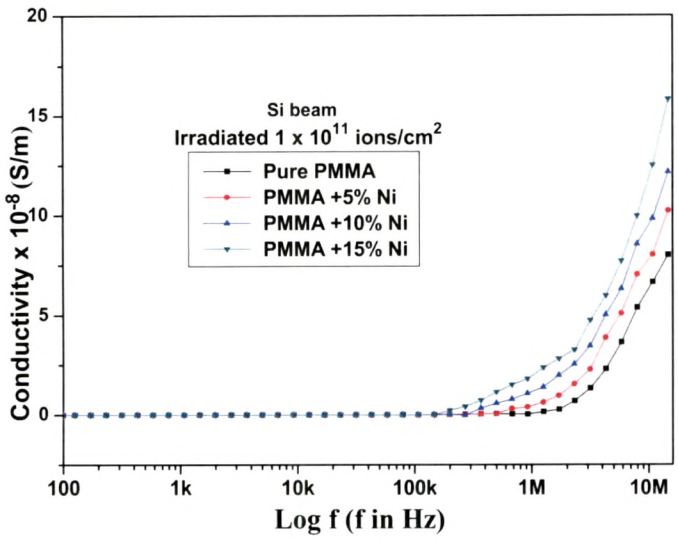

(d)

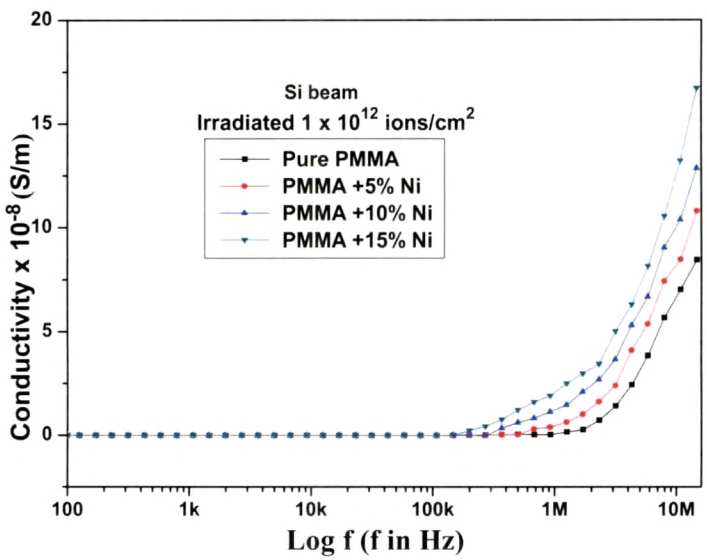

(e)

Fig. 5.7 Conductivity Vs Log f for (a) pristine (b) C beam (1 x 10^{11} ions/cm^2) (c) C beam (1 x 10^{12} ions/cm^2) (d) Si beam (1 x 10^{11} ions/cm^2) (e) Si beam (1 x 10^{12} ions/cm^2)

Dielectric properties of composites:

The dielectric constant showed the ability of a material to store electric potential energy under the influence of an alternative electric field. The effect of nickel concentrations and irradiation on the dielectric constant under various applied sweep

frequencies is shown in Fig. 5.8(a-e). The variation in dielectric constant with frequency indicated the presence of an interfacial polarization in the PMMA matrix. This gradually decreasing dielectric constant with increased frequency is thought to be caused by the slow dielectric relaxation of the matrix and the interface of the composite [23]. At higher frequencies, the periodic reversal of the electric field occurs so fast that there is no excess ion diffusion in the direction of the field. Hence dielectric constant decreases with increasing frequency. The observed behaviour of the fluence dependence of dielectric constant in studied frequency range can be explained by the enhanced free carriers due to irradiation [24].

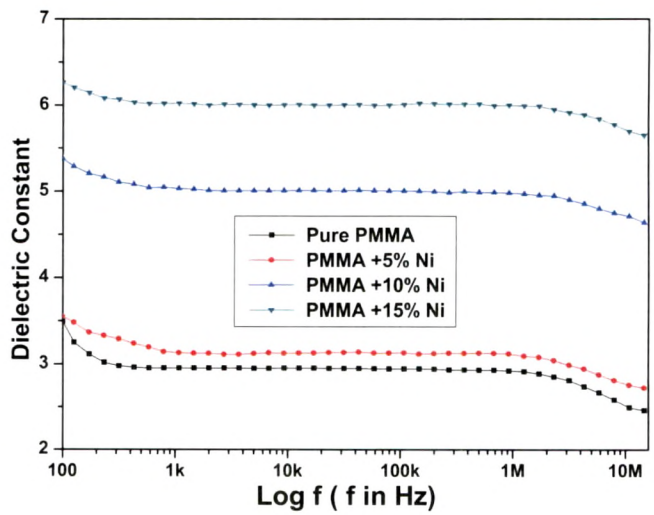

(a)

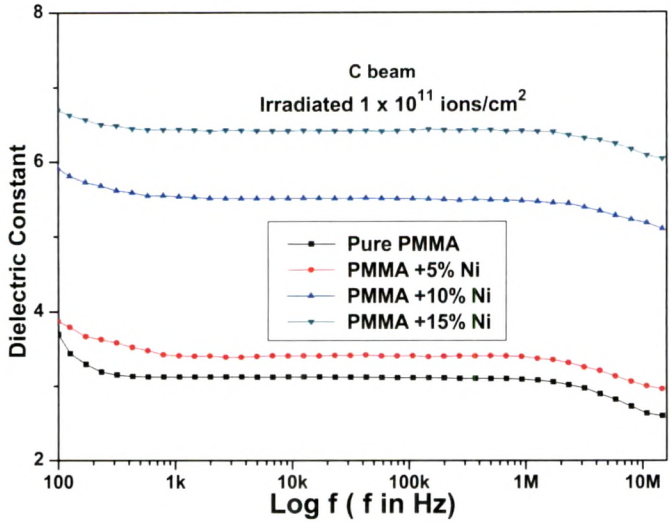
C beam
Irradiated 1 x 10^11 ions/cm^2
Pure PMMA
PMMA +5% Ni
PMMA +10% Ni
PMMA +15% Ni
Dielectric Constant
Log f (f in Hz)
8
6
4
2
100
1k
10k
100k
1M
10M

(b)

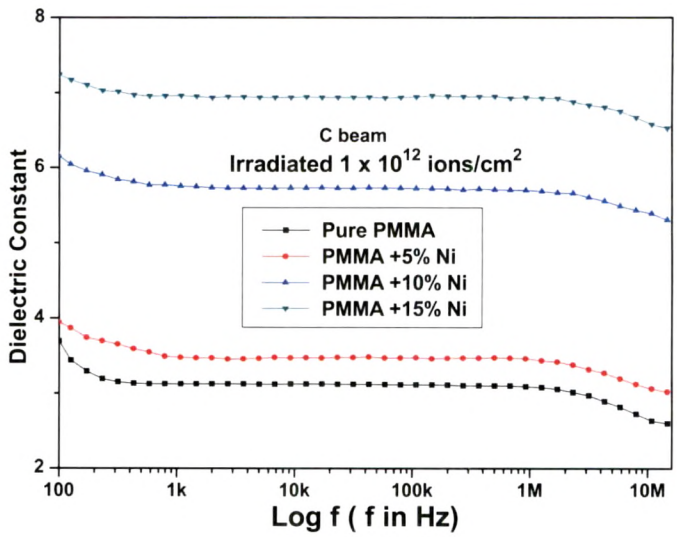
C beam
Irradiated 1 x 10^12 ions/cm^2
Pure PMMA
PMMA +5% Ni
PMMA +10% Ni
PMMA +15% Ni
Dielectric Constant
Log f (f in Hz)
8
6
4
2
100
1k
10k
100k
1M
10M

(c)

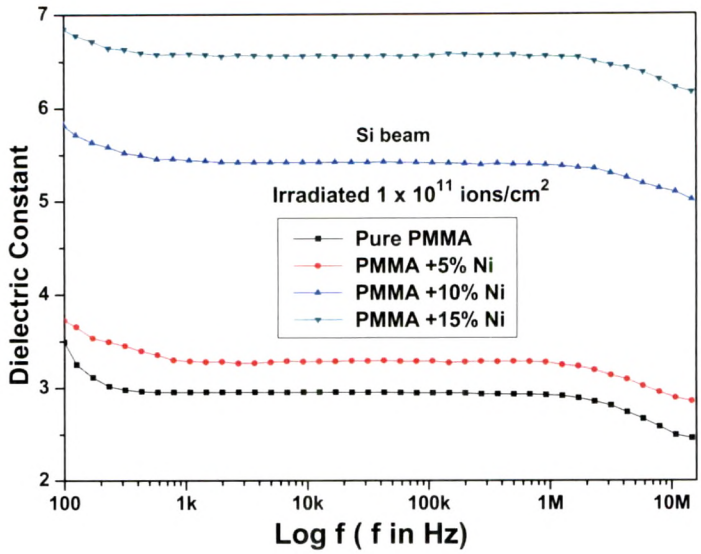

(d)

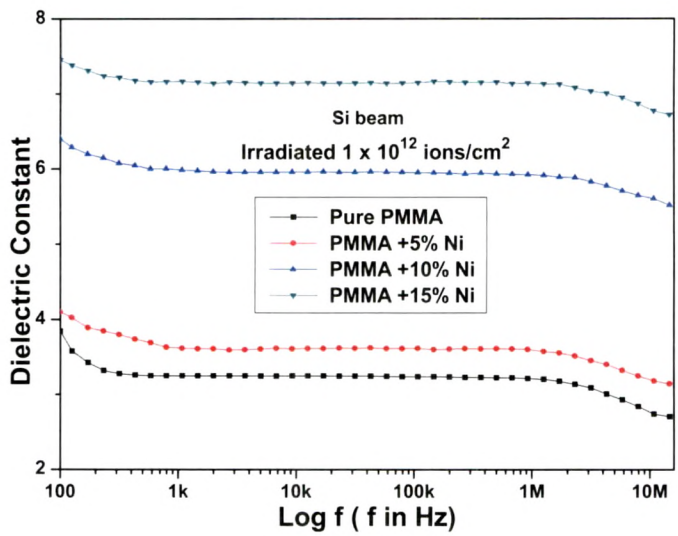

(e)

Fig. 5.8 Dielectric constant Vs Log f for (a) pristine (b) C beam (1 x 10^{11} ions/cm^2) (c) C beam (1 x 10^{12} ions/cm^2) (d) Si beam (1 x 10^{11} ions/cm^2) (e) Si beam (1 x 10^{12} ions/cm^2)

Fig. 5.9(a-e) shows the variation of dielectric loss with log frequency. The dielectric loss decreases exponentially and then became less dependent on frequency. As the frequency increased further, the charge accumulation decreases so the dipole polarization effects reduced, and the value of the loss factor declined accordingly

[25]. The increase in dielectric loss with increasing filler contents may be attributed to the interfacial polarization mechanism of the heterogeneous system. Further, moderate increase in loss occurs due to irradiation. The growth in dielectric loss and thus increase in conductivity is brought by an increase in the conduction of residual current and the conduction of absorption current [23].

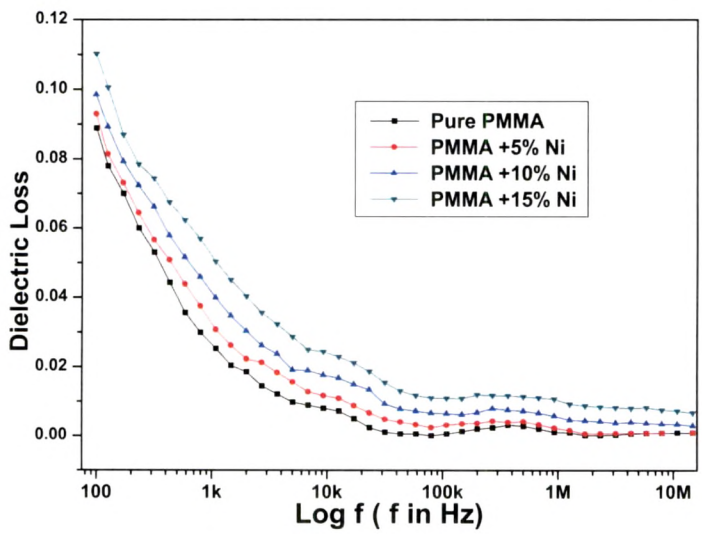

(a)

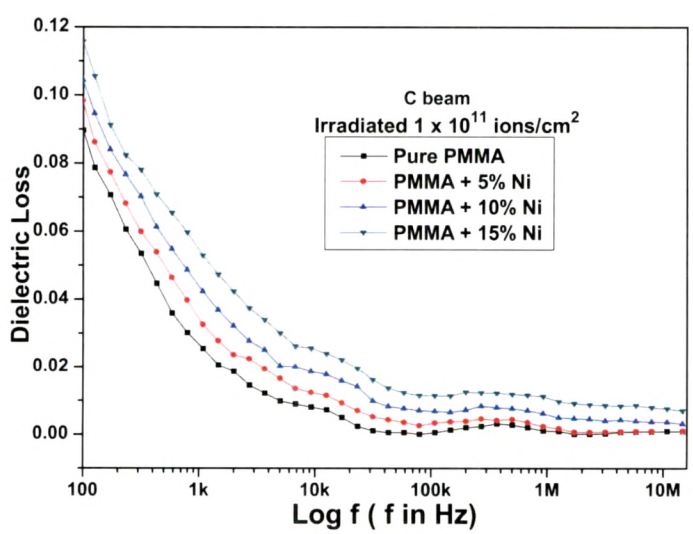

(b)

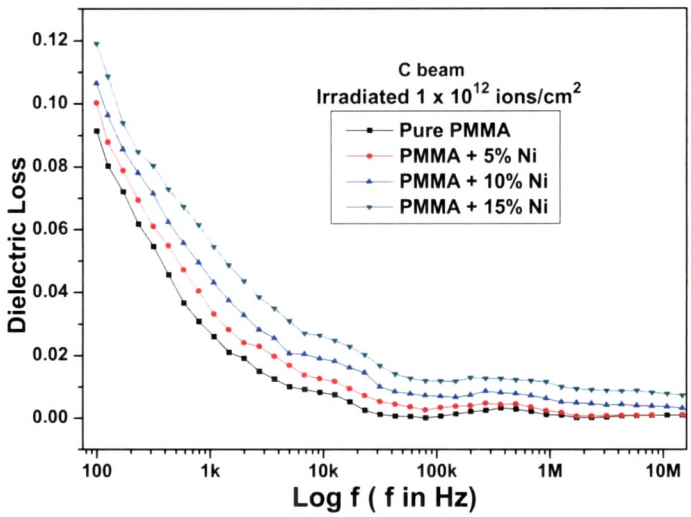
C beam
Irradiated 1 x 10^12 ions/cm^2
Pure PMMA
PMMA + 5% Ni
PMMA + 10% Ni
PMMA + 15% Ni
Dielectric Loss
0.12
0.10
0.08
0.06
0.04
0.02
0.00
100
1k
10k
100k
1M
10M
Log f (f in Hz)

(c)

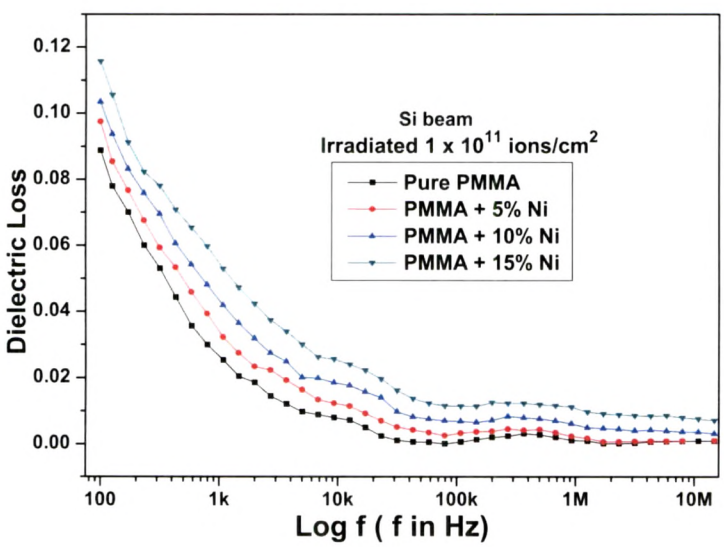
Si beam
Irradiated 1 x 10^11 ions/cm^2
Pure PMMA
PMMA + 5% Ni
PMMA + 10% Ni
PMMA + 15% Ni
Dielectric Loss
0.12
0.10
0.08
0.06
0.04
0.02
0.00
100
1k
10k
100k
1M
10M
Log f (f in Hz)

(d)

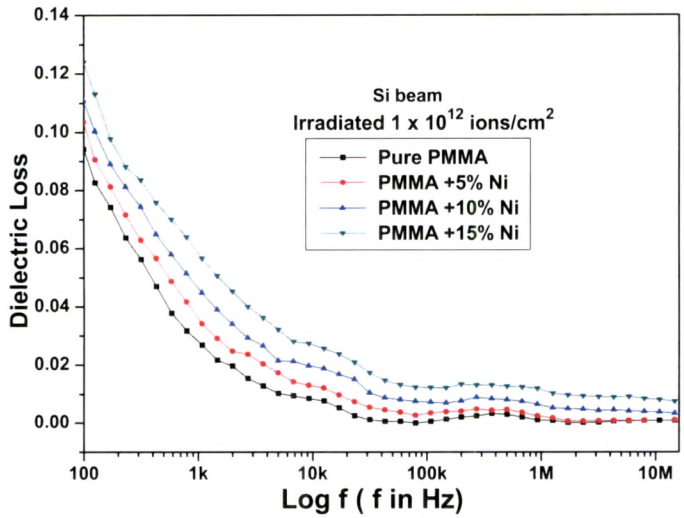

(e)

Fig. 5.9 Dielectric loss Vs Log f for (a) pristine (b) C beam (1 x 10^{11} ions/cm^2) (c) C beam (1 x 10^{12} ions/cm^2) (d) Si beam (1 x 10^{11} ions/cm^2) (e) Si beam (1 x 10^{12} ions/cm^2)

Conclusion:

It was observed from the UV- visible spectroscopy analysis that the band gap value moved to the lower energy (from 4.37 eV upto 3.43 eV) on doping with nickel nanoparticles, as well as upon irradiation. An XRD analysis reveals that the crystallite size of the composites decreased after ion beam irradiation which is also corroborated by the DSC analysis due to the chain scissioning upon irradiation. SEM images showed damages upon ion beam irradiation. The ion beam irradiation of polymer nanocomposites leads to chain scission and cross linking. As a result of that there are changes in magnetic and dielectric properties. The magnetic properties enhanced after irradiation which may be attributed to the exchange dipolar interaction of particles in the matrix and generation of free radicals. AC electrical and dielectric properties of PMMA/Ni nanocomposites were studied over a wide range of frequency as a function of filler concentration. Both the dielectric constant and the electrical conductivity of the composites increased with the increase of Ni content. These phenomena could be

interpreted from interfacial polarization of heterogeneous systems. From the changes observed in composites due to ion beam irradiation, we conclude that the effect of Si-beam is more effective than that of the C-beam because of large energy loss due to heavy ion.

5.2 Effect of swift heavy ions irradiation on PS + Ni nanocomposites:

5.2.1 X-ray diffraction analysis:

The X-ray diffraction patterns of pure Ni (Fig 5.1(a)) and nanocomposites are shown in Fig 5.10. It clearly indicates that nickel is a crystalline but polymer is amorphous in nature and its composite shows semi-crystalline behaviour. The diffraction patterns of the irradiated samples by 85 MeV C ions and 120 MeV Si ions, which exhibited an increase in the peak intensity and a decrease in the full width at half maximum (FWHM) corresponding to all observed peaks of nickel. This behavior may be attributed to cross-linking effect, which may results in the alignment of the polymeric chains. The average crystallite size (t) for pristine and irradiated samples was calculated using Scherrer's formula [11] as dicussed in chapter 2 in section 2.3.1 from the realtion 2.2.3.

$b=K\lambda/L\cos\theta$

where b is FWHM in radians, λ is the wavelength of X-ray beam (1.5418 Å), L is the crystallite size in Å, K is a constant which varies from 0.89 to 1.39, but for most of the cases it is close to 1.

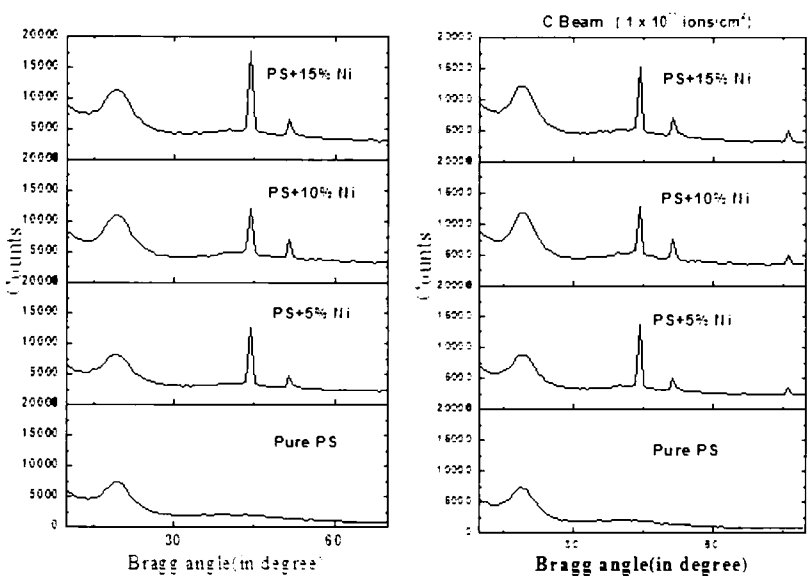

(a) (b)

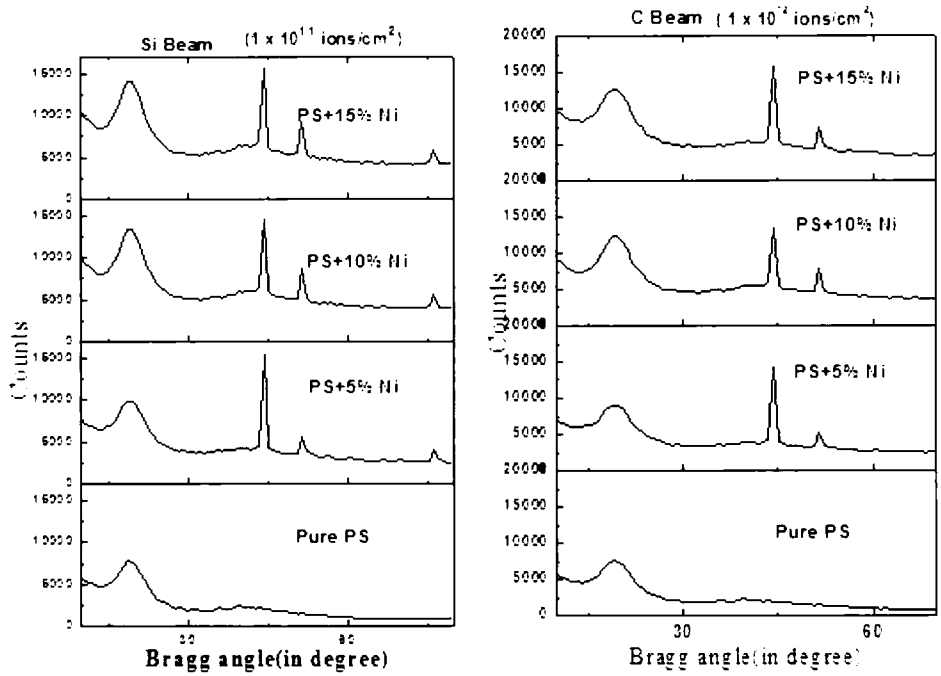

(c) (d)

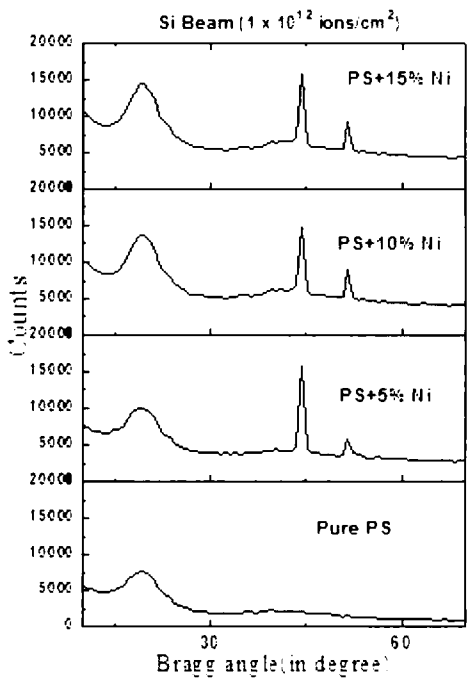

(e)

Fig 5.10 X-ray diffraction patterns of (a) PS+ Ni (pristine) (b) C beam (1 x 10^{11} ions/cm^2) (c) C beam (1 x 10^{12} ions/cm^2) (d) Si beam (1 x 10^{11} ions/cm^2) (e) Si beam (1 x 10^{12} ions/cm^2)

The crystallite size was calculated corresponding to the peak of the pristine and irradiated samples and the results are listed in Table 5.4 [26]. The increase in crystallite size suggested the cross linking mechanism.

Table 5.4 Crystallite size of pristine and irradiated samples

Sample	Pristine		C Beam		Si Beam	
	2θ	Crystallite size (nm)	Crystallite size (nm) ($1x10^{11}$) ions/cm^2	Crystallite size (nm) ($1x10^{12}$) ions/cm^2	Crystallite size (nm) ($1x10^{11}$) ions/cm^2	Crystallite size (nm) ($1x10^{12}$) ions/cm^2
PS+ 5%Ni	44.54	10.21	10.53	10.78	10.98	11.13
	51.24	10.82	10.90	11.02	11.10	11.15
	Average	10.52	10.72	10.89	11.04	11.14
PS + 10%Ni	44.56	10.28	10.67	10.89	11.52	11.87
	51.25	10.89	11.01	11.10	11.67	11.98
	Average	10.58	10.84	10.99	11.60	11.92
PS + 15%Ni	44.60	10.40	10.80	11.50	11.76	11.88
	51.27	11.10	11.56	11.75	12.02	12.24
	Average	10.75	11.18	11.62	11.89	12.06

5.2.2 Thermal response (Differential Scanning Calorimetery (DSC)):

Fig. 5.11 shows the glass transition behavior of polymer matrix and composites. The important property of the glass transition (Tg) of polymer at which, the weak secondary bonds that stick the polymer chains together are broken, and the macromolecule starts to move. The interaction of polymer chains and nanoparticles surface can alter the chain kinetics by decreasing or increasing glass transition temperature of the polymer. Tg of the pure PS is observed at 65.2 °C and those of composite, pristine and irradiated samples at 66.2 °C and 72.5°C respectively with 85 MeV C-ions. Further with 120 MeV Si-ions, we observed that the Tg of irradiated

sample is around 75.68 ^{o}C. The value of Tg for highest fluence is listed in Table 5.5. This behavior probably arises due to branching formed (cross linking

Table 5.5 Values of glass transition for pristine and irradiated composites

Sample name	Tg (Pristine)	Tg (C beam)	Tg (Si beam)
PS + 5 %Ni	65.8	71.9	73.1
PS + 10 %Ni	67.1	73.3	74.5
PS + 15 %Ni	71.5	73.7	75.7

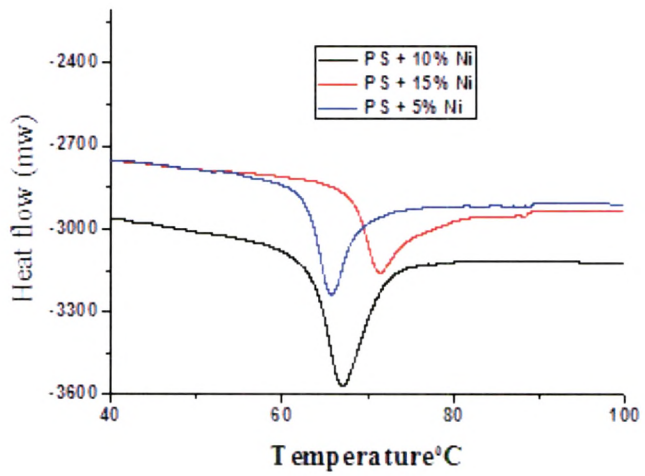

(a)

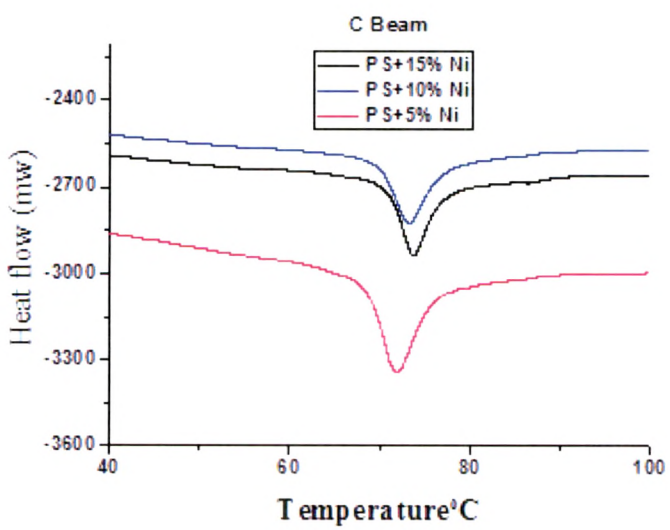

(b)

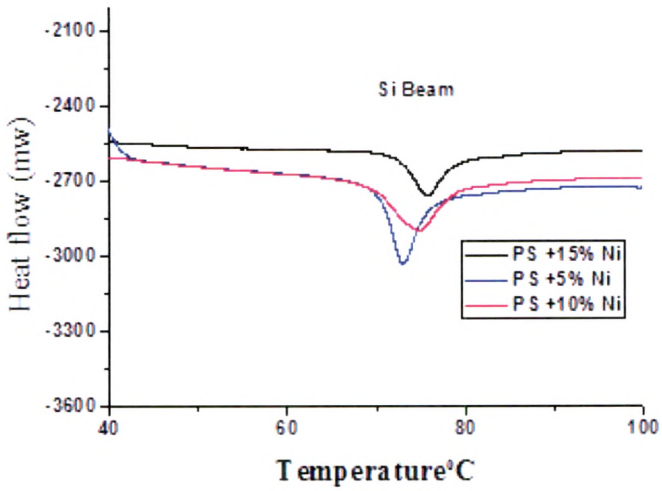

(c)

Fig. 5.11 DSC spectra for (a) Pristine (b) C beam (c) Si beam composites

effect) when islands of nanoparticles are bonded with polymeric chains. This lowers the mobility of the chains, and as a result the glass transition temperature increases in the nanocomposites [27]. So after irradiation, glass transition temperature was shifted further towards higher temperature, this further reveals cross linking between nanoparticles and polymer matrix which is also corroborated with XRD analysis.

5.2.3 Optical response:

The absorption of light energy by polymeric materials in the UV and visible region involves promotion of electrons in the orbital from ground state to the higher energy states. UV–Vis spectroscopy provides valuable information on optical band gap energy (Eg). The electronic transitions (→) that are involved in the ultraviolet and visible regions are of the following type $\sigma \rightarrow \sigma^*$, $n \rightarrow \pi^*$, and $\pi \rightarrow \pi^*$ [27]. The absorbance edge of the UV-Vis spectra of pristine nanocomposites and irradiated by

C and Si ions is shown in Fig 5.12 (a-e). The absorbance in aromatic compounds is due to the π to π^* transition. This is very sensitive to the change in the environment around the phenyl ring [28]. Ion beam interaction with polymers generates damage which leads to the formation of new defects and new charge states. It is observed that optical absorption increases with increasing energy loss and this absorption shifts from UV–Vis to the visible region for all irradiated nanocomposite samples. With increase of electronic energy loss the nanocomposites become gradually opaque to the visible light and the absorption edge shifted from UV to the visible region. The increase in absorption with irradiation may be attributed to the formation of a conjugated system of bonds due to bond cleavage and reconstruction [29]. The shifting of absorption edge towards visible is generally considered to result from carbonization of the material under irradiation [30] which is also corroborated to the dielectric results.

Determination of optical band gap:

Optical feature of the pristine and irradiated samples have been studied by Perkin-Elmer 25 Lambda UV-Visible spectroscope in the frequency range 200-600 cm^{-1} as illustrated in Fig. 5.12 (a-e). The optical band gap E_g is obtained by tauc's equation [17] as described in chapter 2 in section 2.3.3 by relation 2.2.4.

i. e. $\omega\varepsilon(\lambda) = (\hbar\omega - E_g)^2$

Where $\varepsilon(\lambda)$ is the optical absorbance and λ is the wavelength. The intersection of the extrapolated spectrum with the abscissa of the plot $\varepsilon^{1/2}/\lambda$ versus $1/\lambda$ yields the gap wavelength λ_g from which the energy gap is derived as $E_g = hc/\lambda_g$. It is noticed that the band gap (energy gap) value shifted to lower energy from 4.35 eV upto 3.43 eV due to doping of nickel nanoparticles and also upon irradiation with both the ions.

This behavior of the optical gap of ion-irradiated samples can be explained following the model of Robertson and O Reilly [32, 33].

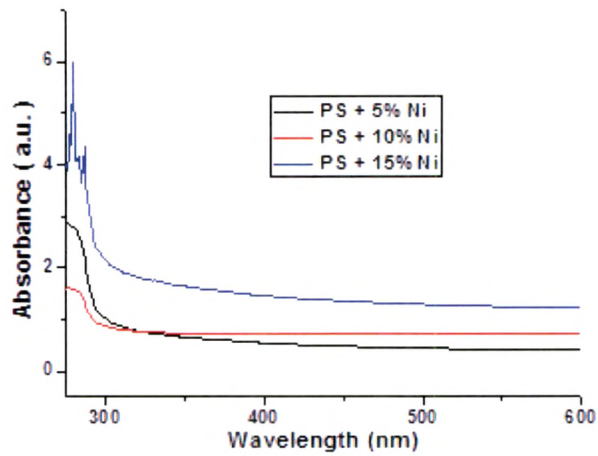

(a)

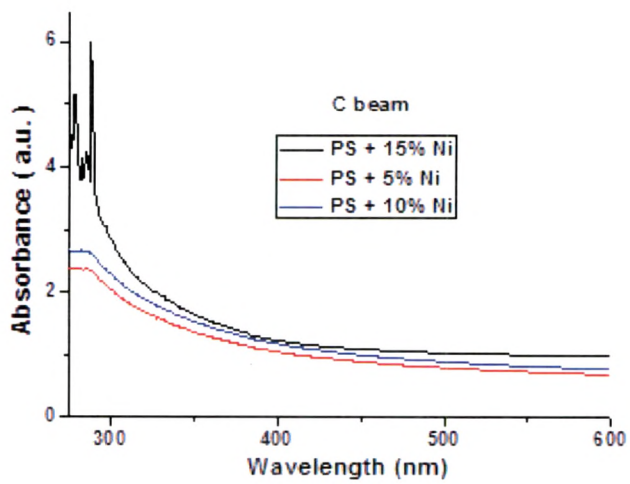

(b)

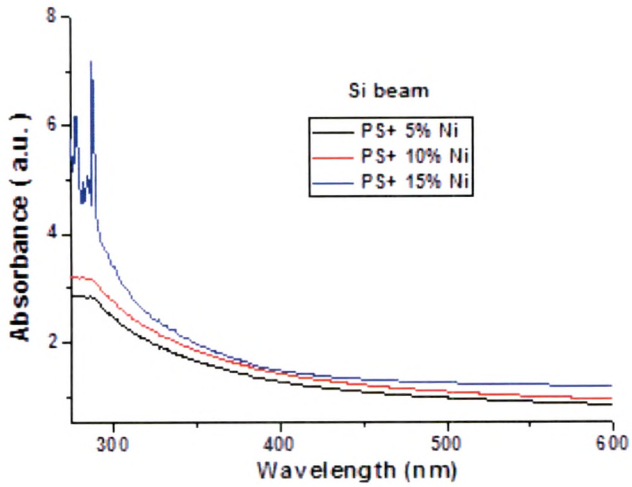

(c)

Fig. 5.12 Absorbance spectra of (a) Pristine (b) C beam (c) Si beam composites

The number of carbon hexagon rings in the cluster (M) is then found from the relation 2.2.6 [32] as discussed in chapter 2 in section 2.3.3.

$$Eg \approx 2\,|\beta|\,\sqrt{M}$$

Where, $|\beta|$ is a bond integral that represents the interaction energy of two π atomic orbitals. A theoretical value for $|\beta|$ proposed by Robertson and O Reilly is 2.9 eV, which according to Compagnini et al. [34] is an overestimation of the true value. So, the best-fit value of $|\beta|$ given by them is 2.2 eV. In the present study on the aromatic polymer, given equation has been used to calculate the value of M and its behaviour with different ions is summarized in Table 5.6. The number of rings (M) reveals constant with the filler and upon irradiation except for Si-ions at a fluence of 1×10^{12} ions/cm^2.

Table 5.6 Band gap by direct allowed transitions, number of carbon atoms in pristine and irradiated composites.

Sample	Pristine		C Beam		Si Beam	
	Band gap in eV	No. of carbon hexagon rings	Band gap in eV	No. of carbon hexagon rings	Band gap in eV	No. of carbon hexagon rings
PS + 5%Ni (1 x 10^{11} ions/cm^2)	4.35	~1	4.30	~1	4.08	~1
PS + 5%Ni (1 x 10^{12} ions/cm^2)	4.32	~1	4.04	~1	3.98	~1
PS + 10%Ni (1 x 10^{11} ions/cm^2)	4.20	~1	3.95	~1	3.88	~1
PS + 10%Ni(1 x 10^{12} ions/cm^2)	4.14	~1	3.88	~1	3.75	~1
PS + 15%Ni (1 x 10^{11} ions/cm^2)	4.12	~1	3.81	~1	3.60	~1
PS + 15%Ni(1 x 10^{12} ions/cm^2)	4.02	~1	3.75	~1	3.43	~2

5.2.4 Surface morphology:

Fig. 5.13(a–c) shows the SEM images of pristine, composites and irradiated composite films with magnification of X250. The analysis shows that the filled partilces are distributed randomly in the matrix which display continuous contact between themselves and formed conducting paths. The surface becomes smoothen upon irradiation.The decrease in roughness with Ni-nanoparticles may be attributed to the decrease in density of metal particles on the surfaces of the films, which is also responsible for increase in crystallinity of the material on irradiations revealed by XRD analysis.

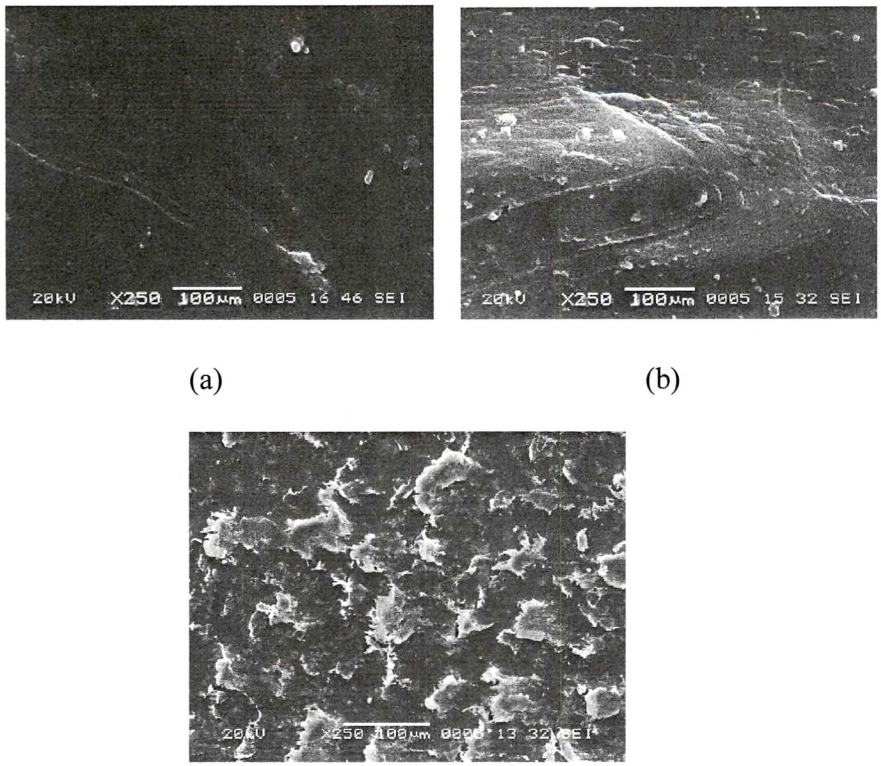

(a) (b)

(c)

Fig. 5.13 SEM images of (a) PS+ 15 % Ni (pristine) (b) PS + 15 % Ni (C beam) (c) PS + 15 % Ni (Si beam)

5.2.5 Magnetic properties:

The static and dynamic magnetic properties were measured by using Quantum Design, over a broad range of magnetic fields. The dc magnetic characteristic was done by using field-cooled-zero-field cooled (FC-ZFC) and M-H hysteresis loop measurements. The FC-ZFC measurements were carried out from 5-300 K at applied field of 500 Oe. Hysteresis measurements were carried out at 300 K with magnetic field swept from 50 kOe to -50 kOe.

The magnetic measurement of Ni/PS nano composites having Ni concentration of 15% by weight is discussed here. The Fig. 5.14 (a, b, c) shows the M-H curves for the pristine and irradiated samples. The magnetic parameters extracted from the

measurements are listed here, saturation magnetization (M_S) ~0.070 emu/gm, coercive field (H_C) ~136 Oe, remnant magnetization (M_R) ~0.014 emu/gm for pristine and M_S ~ 0.097 emu/gm, H_C ~145 Oe, M_R~ 0.019 emu/gm and M_S ~ 0.109 emu/gm, H_C ~155 Oe, M_R~ 0.022 emu/gm for irradiated by 85 MeV C ions and 120 MeV Si ions respectively. The saturation magnetization in nanoparticle system is generally lower than that of the bulk materials and is strongly influenced by the supporting matrix. M_S increases after irradiation may be attributed to the change in exchange and dipolar interactions mediated by the matrix. However unlike the saturation magnetization, the remnant magnetization is also strongly dependent on the inter particles interaction which is governed by the particles inside the polymer matrix [35]. The enhancement in coercive field upon irradiation is also due to the inter particles interaction.

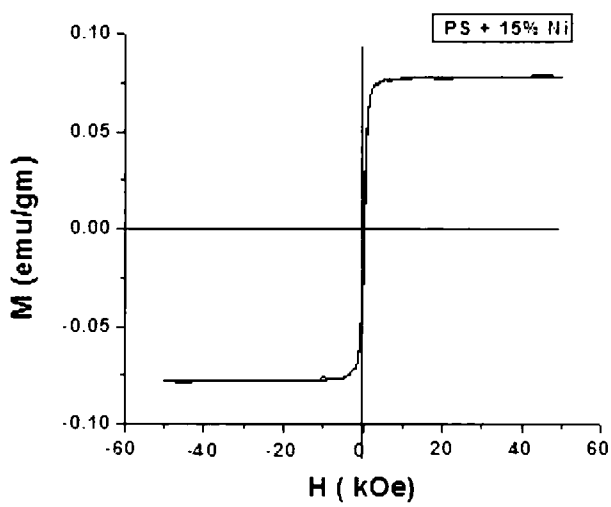

(a)

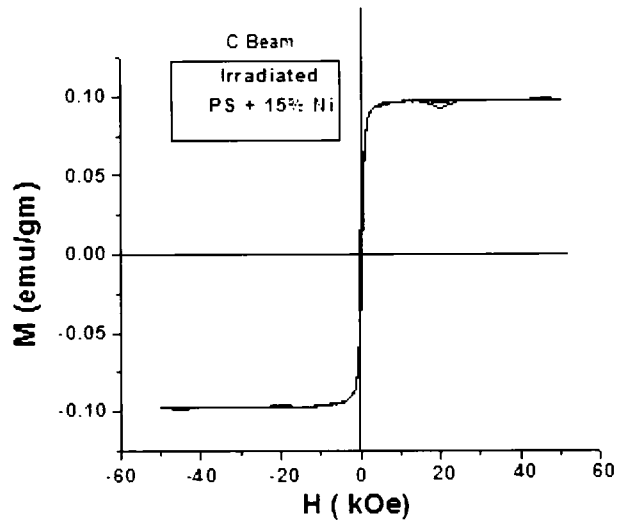

(b)

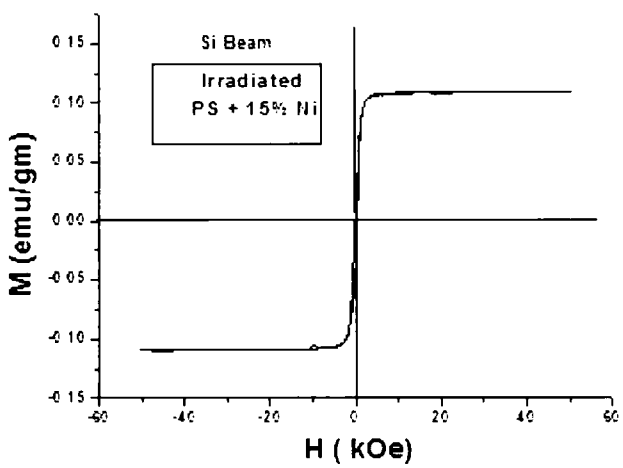

(c)

Fig. 5.14 M-H curves for pristine and irradiated samples

Fig 5.15 shows the comparison of FC-ZFC curves for nanocomposites. For the zero-field-cooled (ZFC) measurements, the sample was cooled down from room temperature to 5 K in the absence of an external magnetic field and the magnetic data were acquired during the warming run in a constant external field. In the field-cooled

(FC) measurements, the samples were initially cooled down to 5 K in the presence of a magnetic field and the FC data were recorded during the warm up cycle in the same magnetic field. The FC–ZFC measurements were carried out in the temperature range 5–300 K at applied field of 500 Oe as shown in Fig. 5.15 for pristine and irradiated samples, respectively. None of these curves show any characteristic sharp change in

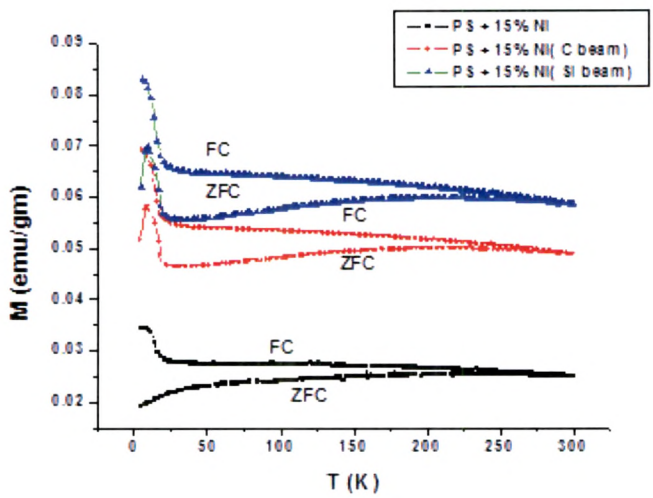

Fig. 5.15 ZFC-FC curves for pristine and irradiated samples

magnetization associated with the well established ferromagnetic to super paramagnetic transition in single domain nanoparticles. This indicates that the particles (mostly in clusters) in the polymer matrix are predominantly ferromagnetic [22]. Magnetization was increased upon irradiation which may be attributed to the creation of free radicals and interaction of particles mediated by the matrix which is also corroborated with the M-H measurements.

5.2.6 AC electrical frequency response:

Conductivity: The conductivity behavior of the PS/Ni nanocomposite films depends on the concentration of the nickel nano particles under an ac field as shown in Fig. 5.16 (a-e). The conductivity of nanocomposite films increases with increasing

nanoparticles loading, while the influence of frequency on the conductivity is stronger than the influence of the concentration of nano-Ni particles, which shows a strong dependence of the conductivity at higher frequency range. Charge carriers are transported mainly through the amorphous phase. The impurity content in the amorphous region is hop to increase with the increasing concentration of nano-Ni particles. The electronic charge carriers transport will be simpler due to the function of impurity and resulting in an increase in the sample conductivity. The conductivity is influenced by the hopping processes of charge carriers in a material and barrier height. The disordered morphology causes the ac mobility to increase with the frequency of the applied electric field and was found to be strongly frequency dependent. Therefore hopping carriers transport became easier, resulting in an increase in conductivity of the films [36]. It is also examined that the conductivity increases upon irradiation. Irradiation is supposed to endorse the metal-polymer bonding and convert it into the hydrogen depleted carbon network due to the emission of hydrogen and/or other volatile gases. It is this carbon network that is believed to make the polymers more conductive [37].

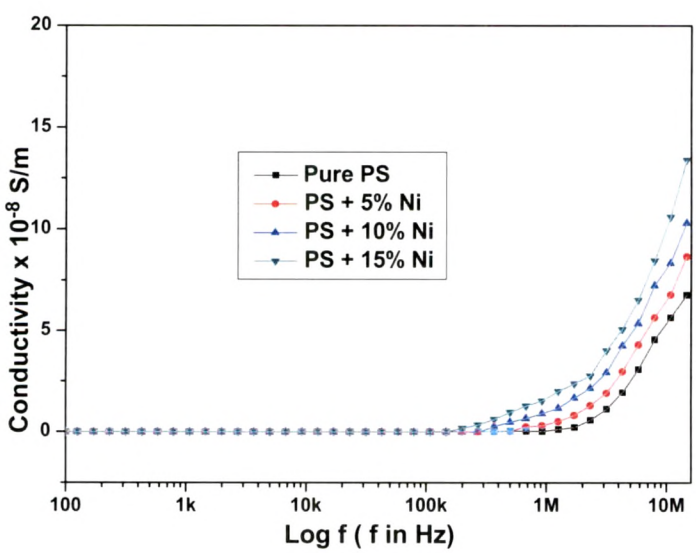

(a)

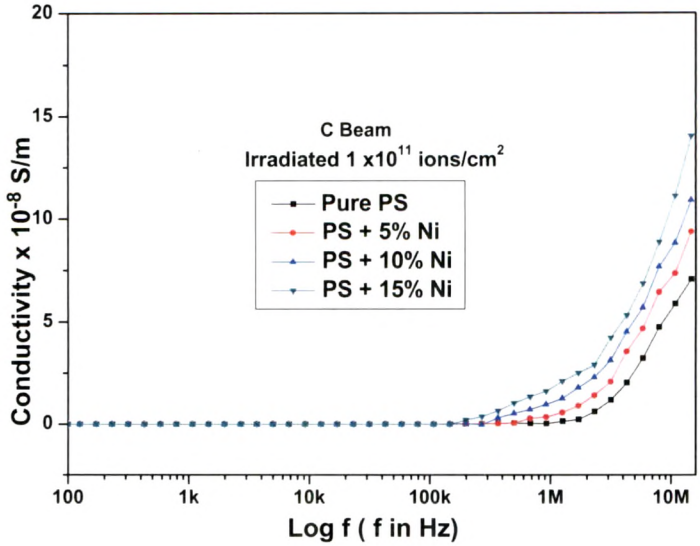
C Beam
Irradiated 1 x10^11 ions/cm^2
Pure PS
PS + 5% Ni
PS + 10% Ni
PS + 15% Ni
Conductivity x 10^-8 S/m
Log f (f in Hz)
20
15
10
5
0
100
1k
10k
100k
1M
10M

(b)

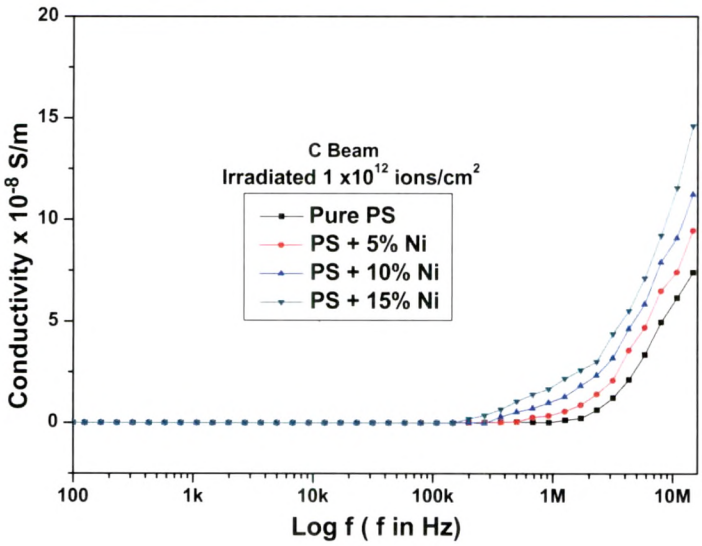
C Beam
Irradiated 1 x10^12 ions/cm^2
Pure PS
PS + 5% Ni
PS + 10% Ni
PS + 15% Ni
Conductivity x 10^-8 S/m
Log f (f in Hz)
20
15
10
5
0
100
1k
10k
100k
1M
10M

(c)

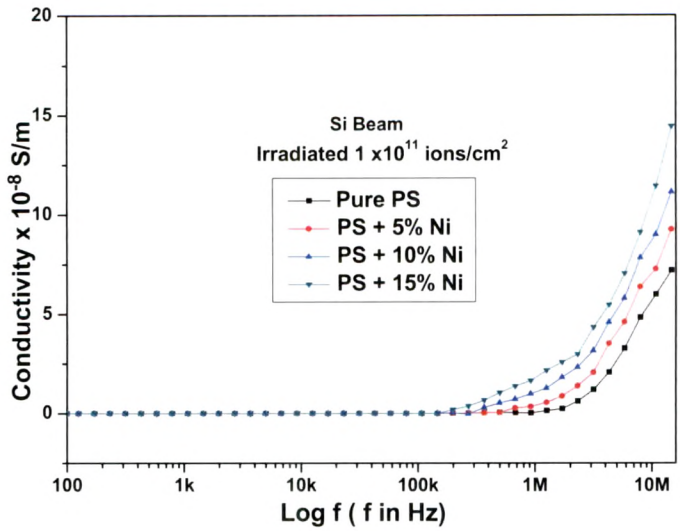

(d)

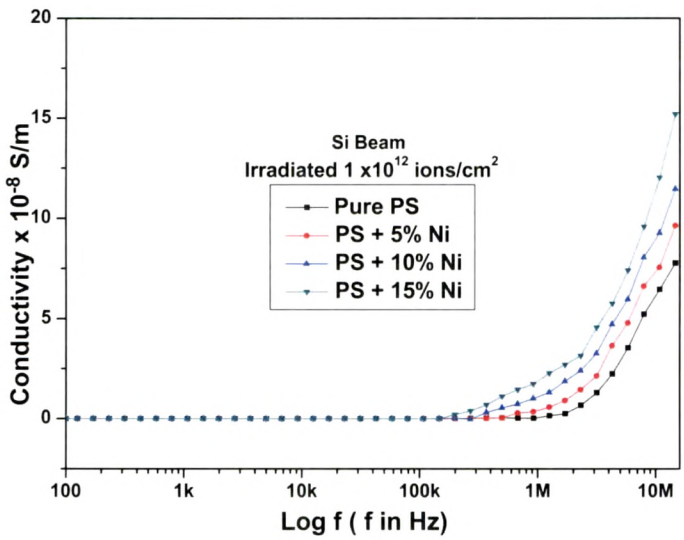

(e)

Fig. 5.16 Conductivity Vs Log f for (a) pristine (b) C beam (1 x 10^{11} ions/cm^2) (c) C beam (1 x 10^{12} ions/cm^2) (d) Si beam (1 x 10^{11} ions/cm^2) (e) Si beam (1 x 10^{12} ions/cm^2)

Dielectric properties of composites:

As can be seen in Fig 5.17(a-e), the value of the dielectric permittivity for PS/Ni nanocomposites depends both on the measuring frequency and the nanofiller concentration. Especially, the dielectric behaviors of PS/Ni nanocomposites with different nickel nanoparticles concentrations in the low frequency range are found to

be increased which is due to the interfacial space charge polarization. The higher the nanofiller loading level, the larger the total effective area of the interfaces between the polymer matrix and the filler, and the thinner the insulating spacers separating nickel nanoparticles, resulting in the considerable increment of the interfacial space-charge

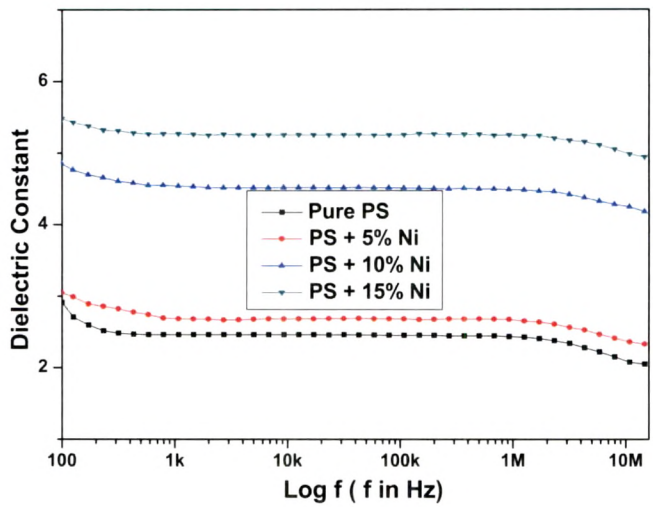

(a)

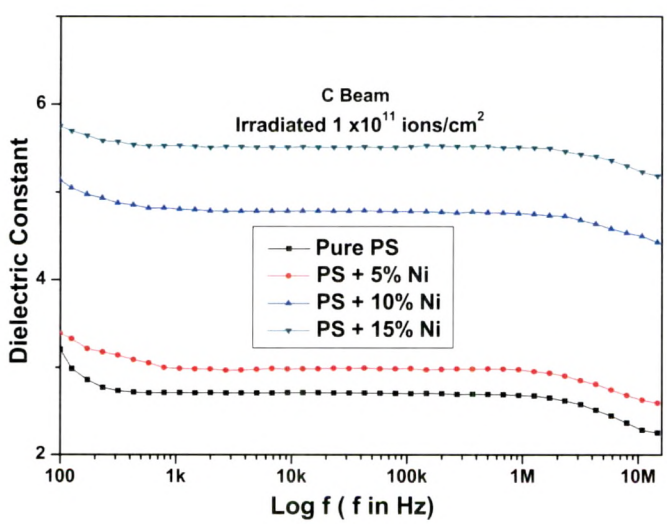

(b)

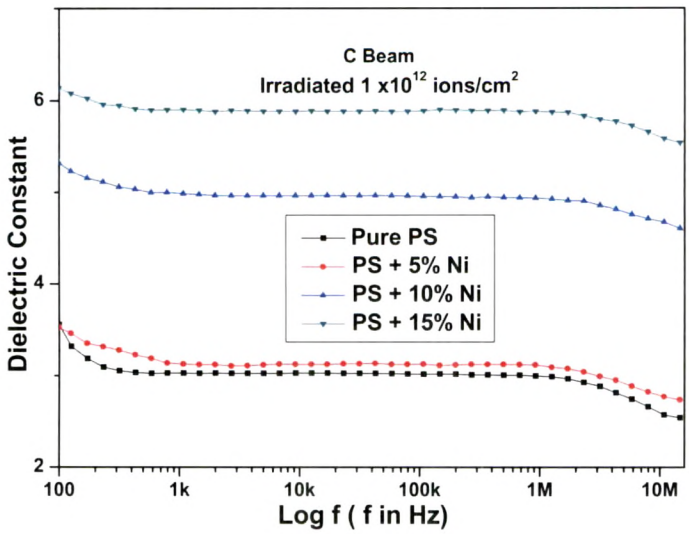
C Beam
Irradiated 1 x10^12 ions/cm^2
Dielectric Constant
Log f (f in Hz)
Pure PS
PS + 5% Ni
PS + 10% Ni
PS + 15% Ni
2
4
6
100
1k
10k
100k
1M
10M

(c)

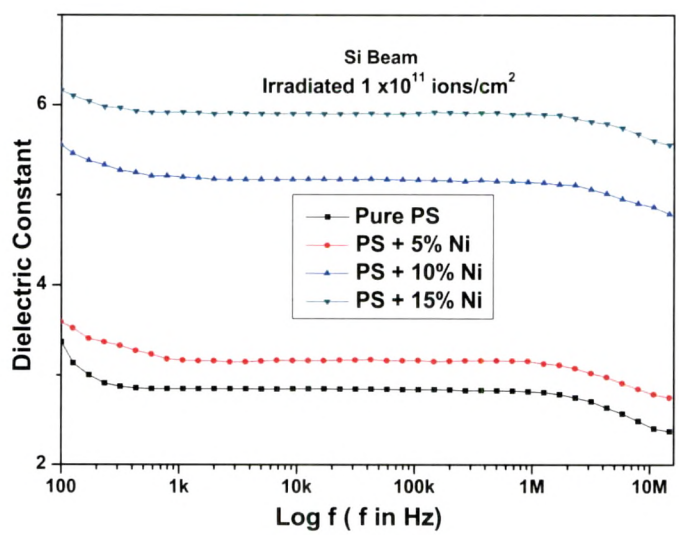
Si Beam
Irradiated 1 x10^11 ions/cm^2
Dielectric Constant
Log f (f in Hz)
Pure PS
PS + 5% Ni
PS + 10% Ni
PS + 15% Ni
2
4
6
100
1k
10k
100k
1M
10M

(d)

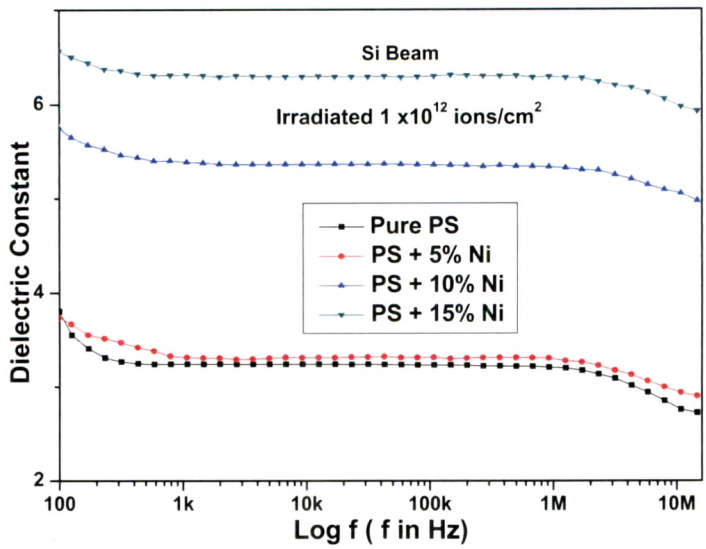

(e)

Fig. 5.17 Dielectric Constant Vs Log f for (a) pristine (b) C beam (1 x 10^{11} ions/cm^2) (c) C beam (1 x 10^{12} ions/cm^2) (d) Si beam (1 x 10^{11} ions/cm^2) (e) Si beam (1 x 10^{12} ions/cm^2)

polarization at these frequency range [36]. As observed from figure, the dielectric constant remains almost constant up to 100 kHz. At these frequencies, the motion of free charge carriers assumed to be constant through the polymer. It is also observed that dielectric constant increases upon irradiation. The increase in dielectric constant may be attributed to the chain scission, cross linking and as a result the increase in the number of free radicals, unsaturation etc. At higher frequency regions, (i.e., beyond 100 kHz), the charge carriers migrate through the dielectric and get trapped against a defect sites and induced an opposite charge in its vicinity. So, the polarization of trapped and bound charges cannot take place and that reduced the dielectric constant [38].

Fig. 5.18(a-e) shows the variation of dielectric loss with log frequency for pristine and irradiated samples of pure PS and nickel nanoparticles dispersed PS films at different concentrations. In general, the dielectric loss of the dielectric material causes

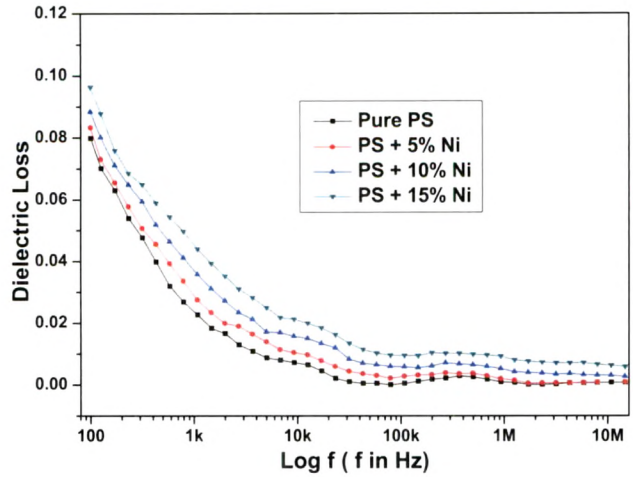
Dielectric Loss
0.12
0.10
0.08
0.06
0.04
0.02
0.00
100
1k
10k
100k
1M
10M
Log f (f in Hz)
Pure PS
PS + 5% Ni
PS + 10% Ni
PS + 15% Ni

(a)

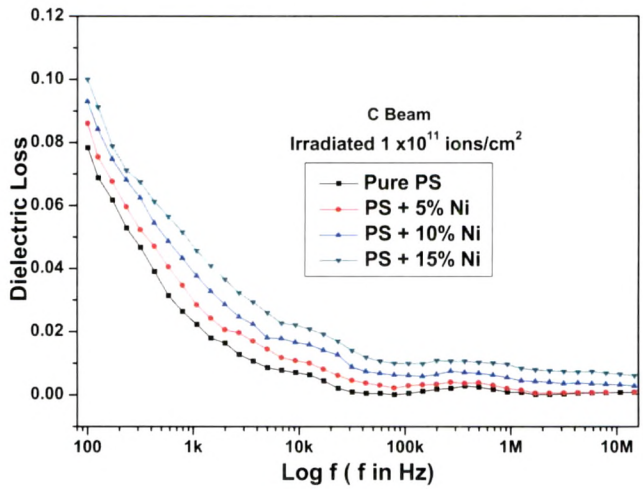
Dielectric Loss
0.12
0.10
0.08
0.06
0.04
0.02
0.00
100
1k
10k
100k
1M
10M
Log f (f in Hz)
C Beam
Irradiated 1 x10^11 ions/cm^2
Pure PS
PS + 5% Ni
PS + 10% Ni
PS + 15% Ni

(b)

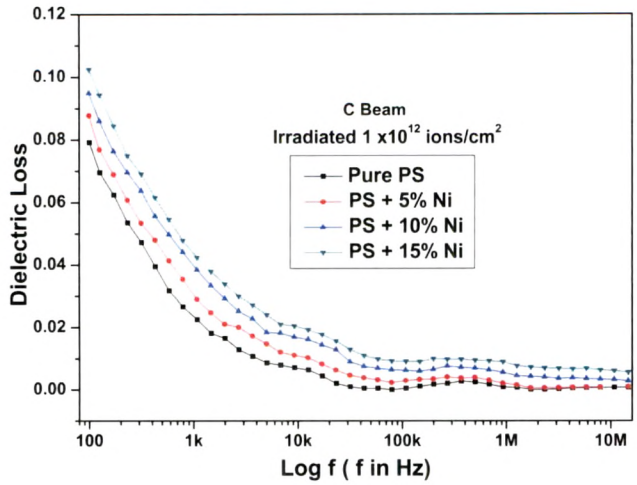
C Beam
Irradiated 1 x10^12 ions/cm^2
Pure PS
PS + 5% Ni
PS + 10% Ni
PS + 15% Ni
Dielectric Loss
Log f (f in Hz)
0.12
0.10
0.08
0.06
0.04
0.02
0.00
100
1k
10k
100k
1M
10M

(c)

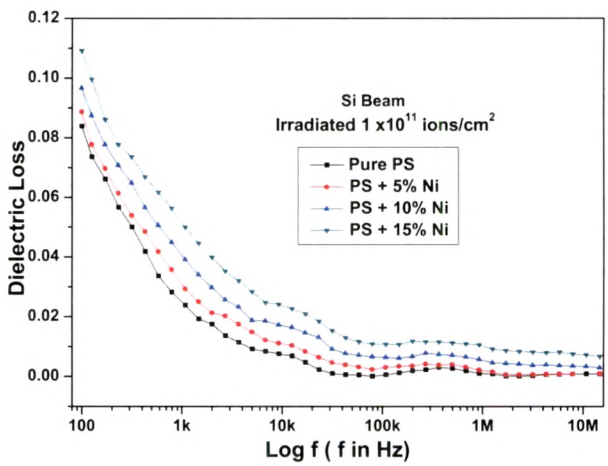
Si Beam
Irradiated 1 x10^11 ions/cm^2
Pure PS
PS + 5% Ni
PS + 10% Ni
PS + 15% Ni
Dielectric Loss
Log f (f in Hz)
0.12
0.10
0.08
0.06
0.04
0.02
0.00
100
1k
10k
100k
1M
10M

(d)

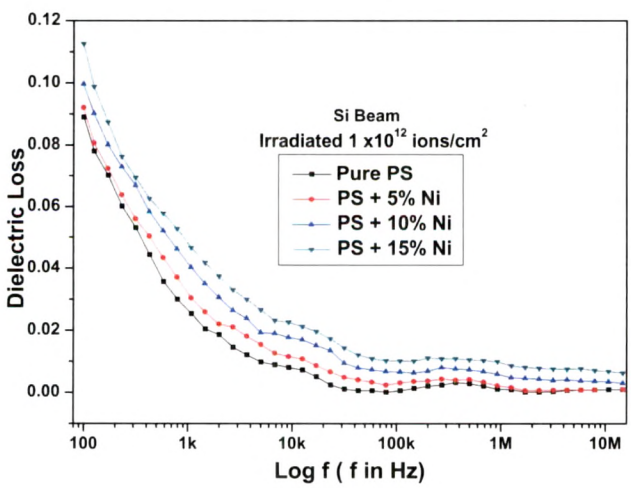
Si Beam
Irradiated 1 x10^12 ions/cm^2
Pure PS
PS + 5% Ni
PS + 10% Ni
PS + 15% Ni
Dielectric Loss
Log f (f in Hz)
0.12
0.10
0.08
0.06
0.04
0.02
0.00
100
1k
10k
100k
1M
10M

(e)

Fig. 5.18 Dielectric loss Vs Log f for (a) pristine (b) C beam (1×10^{11} ions/cm^2) (c) C beam (1×10^{12} ions/cm^2) (d) Si beam (1×10^{11} ions/cm^2) (e) Si beam (1×10^{12} ions/cm^2)

from distortional, dipolar, interfacial, and conduction loss. The dielectric loss decreases moderately with the increase of log frequency as shown in figure. It is observed that dielectric loss increases moderately with the concentration of filler and also with the fluence which may be featured by the interfacial polarization mechanism of the heterogeneous system [39].

Conclusion:

The ion beam irradiation of polymer nanocomposites leads to chain scission and cross linking. As a result of that there are changes in physical properties of composites. It is observed that the crystalline size increased upon irradiation as revealed from XRD analysis. This might be featured to rupture of some polymeric bonds, which is also confirmed by DSC analysis. The magnetic properties enhanced after irradiation which may be attributed to the exchange dipolar interaction of particles in the matrix and generation of free radicals. The AC electrical studies signify that the conductivity increases on increasing the frequency and also upon irradiation. Dielectric constant is observed to change upon irradiation. This might be attributed to breakage of chemical bonds and resulting in the increase of free radicals, unsaturation, etc.

5.3 Summary:

Two different composites have been studied using two different ion beams (C and Si - ions) irradiations. Structural, optical, thermal, magnetic properties, electrical properties and surface morphology have been examined by different characterization techniques.

XRD analysis; the results show that the crystallite size of fillers decreases slightly upon both ion beams irradiations in PMMA nanocomposites. It is also observed that the intensity of the peak decreases and to some extent broadening of the peak after irradiation offers confirmation of decrease in crystallinity. Since no significant change in the peak position is observed, this reveals that lattice parameters do not change significantly in both ion beams irradiations. Rather in the case of PS nanocomposites, crystallite size of fillers increases upon both ion beams irradiations which may be attributed to cross linking effect.

DSC thermograms; the Tg value decreases upon irradiations in PMMA nanocomposites and increases upon irradiations in PS composites. This behavior probably arises due to branching (cross-linking effect) when islands of nanoparticles are bonded with polymeric chains. This lowers the mobility of the chains, and as a result, the glass transition temperature increases in the nanocomposites. Decrease in Tg was explained by thin film model. When the inter-particles distance is small enough, then the polymer between two particles can be considered as a thin film. Assuming that there is small or no interfacial interaction between the filler and matrix exists and then Tg decreases.

UV-Vis analysis; the band gap values for both composites were increased upon concentration of fillers and both ions irradiations. It was observed from the UV-visible spectroscopy analysis that the band gap value moved to the lower energy.

Surface morphology; SEM images showed that increase in density in PMMA nanocomposites and decrease in density in PS nanocomposites upon irradiations.

Dielectric analysis; Ac electrical conductivity of all pristine and irradiated samples at different filler concentrations is shown in Fig.5.19. The conductivity of nanocomposite films increases with increasing nanoparticles loading, while the influence of frequency on the conductivity is stronger than the influence of the concentration of nano-Ni particles, which shows a strong dependence of the conductivity at higher frequency range. Charge carriers are transported mainly through the amorphous phase. The impurity content in the amorphous region is hop to increase with the increasing concentration of nano-Ni particles. The electronic charge carriers transport will be simpler due to the function of impurity and resulting in an increase in the sample conductivity. The conductivity is influenced by the hopping processes of charge carriers in a material and barrier height. The disordered morphology causes the ac mobility to increase with the frequency of the applied electric field and was found to be strongly frequency dependent. Therefore hopping carriers transport became easier, resulting in an increase in conductivity of the films. Conductivity is further observed to increase upon irradiation. Irradiation is expected to promote the metal to polymer bonding and convert polymeric structure into hydrogen depleted carbon network. It is this carbon network that is believed to make the polymer more conductive. Fig. 5.20 shows comparison of conductivity of all composites before and after irradiation. For the sake of comparison filler concentration (5, 10, 15 wt%) at a fluence of 1 x 10^{12} ions/cm^2 for C and Si ions beam

at a frequency 10 MHz have considered. Similar study for dielectric constant of all composites has been done and shown in Fig 5.20 at a frequency of 10 MHz.

Dielectric loss was studied for all pristine and irradiated samples and result shows frequency and fluence dependent behaviour for all cases. In general, the natures of the curves of electrical response for all samples are same but the magnitude varies with filler material.

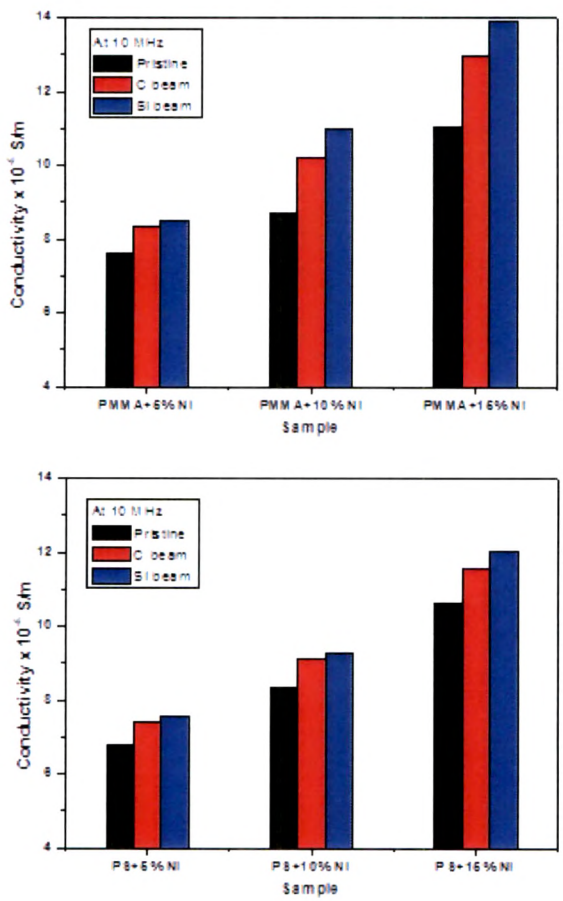

Fig. 5.19 Comparison of conductivity of pristine and irradiated samples at 10 MHz

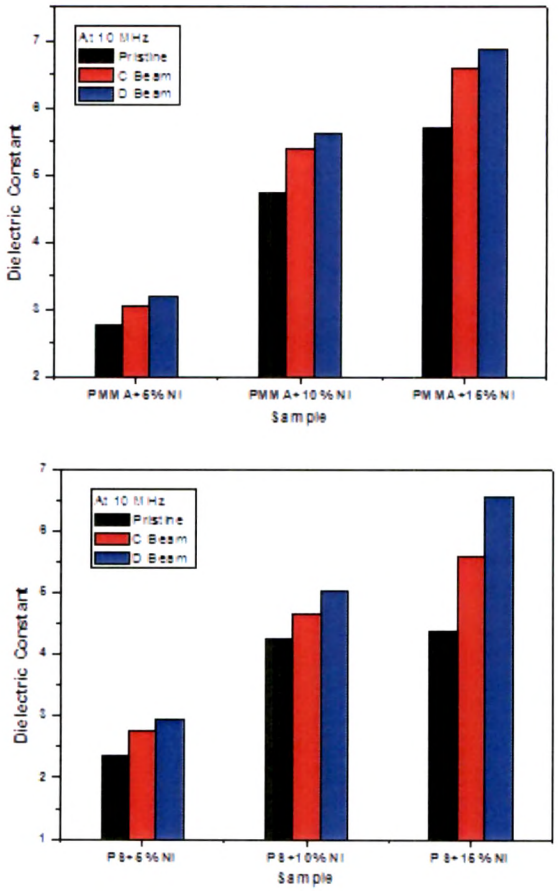

Fig. 5.20 Comparison of dielectric constant of pristine and irradiated samples at 10 MHz

References

[1] D. R. Sharma , Rashi Mathur , S.R. Vadera , N. Kumar , T.R.N. Kutty, Journal of Alloys and Compounds 358 (2003) 193-204.

[2] Xingyi Huang, Chonung Kim, Pingkai Jiang, Yi Yin, Zhe Li, Journal of Applied Physics 105 (2009) 014105 (10 pages).

[3] F. C. Fonseca, G. F. Goya, R. F. Jardim, R. Muccillo, N. L. V. Carren˜o, E. Longo, E. R. Leite, Physical Review B 66 (2002) 104406-104410.

[4] K. Akamatsu, K. Nakahashi, S. Ikeda, H. Nawafune, Eur. Phys. J. D 24 (2003) 377–380.

[5] N L Singh, Anjum Qureshi, A K Rakshit And D K Avasthi, Bull. Mater. Sci. 29(6) (2006) 605-609.

[6] C.J. Bedell, C.J. Solfield, L.B. Bridwell, I.M. Brown, J. Appl. Phys. 67 (1990) 1736-1740.

[7] V. Hnatowicz, J. Kvitek, V. Svorcik, V. Rybka, Appl. Phys. A 58 (1994) 349-352.

[8] N. L. Singh, Chaitali Gavade, P. K. Khanna, Defect and Diffusion Forum,341 (2013) 51-68.

[9] Chaitali Gavade, N. L. Singh, P. K. Khanna, Sunil Shah, Sanjeev Kumar, Advance materials letters (communicated).

[10] R. Kumar, U. De, R. Prasad, Nucl. Instrum. Methods B 248 (2006) 279-283.

[11] P. Scherrer, Gott Nachar, 2 (1918) 98–100.

[12] N. L. Singh, D. Singh, A. Qureshi, Radiation Effects & Defects in Solids 66(8-9) (2011) 640–647.

[13] A. Semwal, A. Negi, R. G. Sonkawade, J. M. S. Rana, R. C. Ramola, Indian J of pure and App Phy 48 (2010) 496-499.

[14] H S Virk , P S Chandi And A K Srivastava, Bull. Mater. Sci. 24(5), 529 (2001)

[15] L. Singh, K. Singh Samra, Radiation Physics and Chemistry 77 (2008) 252–258.

[16] A. Das, S. Dhara and A. Patnaik Physical Rev B 59 (1999) 11069.

[17] Anjum Qureshi , Dolly Singh , N.L. Singh, S. Ataoglu , Arif N. Gulluoglu , Ambuj Tripathi ,D.K. Avasthi, Nuclear Instruments and Methods in Physics Research B 267 (2009) 3456.

[18] A. K. Srivastava, H. S. Virk, J. Polym. Mater., 17 (2000) 325.

[19] S. Shah, N.L. Singh, A. Qureshi, D. Singh, K.P. Singh, V. Shrinet, A. Tripathi, Nucl. Instrum. Methods B 226 (2008) 1768.

[20] R. Vijaya Kumar, Yu. Koltypin, O. Palchik, A. Gedanken, Journal of Applied Polymer Science 86 (2002) 160–165.

[21] S. Manna, A. K. Deb, J. Jagannath, and S. K. De, J. Phys. Chem. C 112 (29) (2008) 10659-10662.

[22] Chaitali Gavade, N. L. Singh, D. K. Avasthi, Alok Banerjee, Nuclear Instruments and Methods in Physics Research B, 268 (2010) 3127–3131.

[23] P. Balaji Bhargav, B. A. Sarada, A. K. Sharma And V.V. R. N. Rao, Journal of Macromolecular Science, Part A: Pure and Applied Chemistry 47 (2010) 131–137.

[24] N. L. Singh, S. Shah, A. Qureshi, A Tripathi, F Singh, D. K. Avasthi, P. M. Raole, Bull. Mater. Sci.34(1) (2011) 81–88.

[25] T. Phukan, D. Kanjilal, T. D. Goswami, Nucl. Instr. And Meth. B, 234 (2005) 520.

[26] D. Singh, N.L. Singh, A. Qureshi, P. Kulriya, A. Tripathi, D.K. Avasthi, A.N. Gulluoglu, J. Non-Cryst. Solids, 356 (2010) 856–863.

[27] X. Yan, T. Xu, S. Xu, S. Wang, Nanotechnology, 15 (2004) 1759–1762.

[28] Rajesh Kumar, S. Asad Ali, A.K. Mahur, H.S. Virk, F. Singh, S.A. Khan, D.K. Avasthi, Rajendra Prasad, Nuclear Instruments and Methods in Physics Research B 266 (2008) 1788–1792.

[29] S. Saravanana, M.R. Anantharaman, S. Venkatachalam, D.K. Avasthi, Vacuum 82 (2008) 56–60.

[30] L.S. Farenza, R.M. Papaleo, A. Hallen, M.A. Araujo, R.P. Livi, B.U.R. Sundqvist, Nucl. Instr. and Meth. B 105 (1995) 134.

[31] Zhiyong Zhu, Yunfan Jin, Changlong Liu, Youmei Sun, Mingdong Hou, Chonghong Zhang, Zhiguang Wang, Jie Liu, Xiaoxi Chen, Baoquan Li, Yanbin Wang, Nuclear Instruments and Methods in Physics Research B 169 (2000) 83-88.

[32] J. Robertson, E.P. O Reilly, Phys. Rev. B 35 (1987) 2946.

[33] Lakhwant Singh, Kawaljeet Singh Samra, Ravinder Singh, Nuclear Instruments and Methods in Physics Research B 255 (2007) 350–356.

[34] G. Sui, S. Jana, W. H. Zhong, M. A. Fuqua, C. A. Ulven, Acta Mater., 56 (2008) 2381–2388.

[35] J. L. Wilson, P. Poddar, N.A. Frey, H. K. Srikanth, J. P. Mohomed, H. Kotha, S. J. Wachsmuth, J. Appl. Phys., 95 (2004) 1439-1443.

[36] X Y Huang, P K Jiang, C U Kim, Journal of Applied Physics, 102 (2007) 124103-8.

[37] A.Qureshi, N.L. Singh, S. Shah, F. Singh, D. K. Avasthi, Journal of Macromolecular Science, Part A: Pure and Applied Chemistry, 45 (2008) 265-270.

[38] A. K. Jonscher, Dielectric Relaxation in Solids; Chesla Dielectric Press: London, 1983.

[39] N. L. Singh, S.Shah, A. Qureshi, K. P. Singh, V. Shrinet, A. Tripathi, Radiat. Eff. Def. Solids, 163 (2) (2008) 169–177.